WNT signaling drives cholangiocarcinoma growth and can be pharmacologically inhibited

Luke Boulter,[1,2] Rachel V. Guest,[1] Timothy J. Kendall,[2,3] David H. Wilson,[2] Davina Wojtacha,[1] Andrew J. Robson,[1] Rachel A. Ridgway,[4] Kay Samuel,[1] Nico Van Rooijen,[5] Simon T. Barry,[6] Stephen J. Wigmore,[3] Owen J. Sansom,[4] and Stuart J. Forbes[1,3]

[1]MRC Centre for Regenerative Medicine, Scottish Centre for Regenerative Medicine, Edinburgh, United Kingdom. [2]MRC Human Genetics Unit, Western General Hospital Campus, Edinburgh, United Kingdom. [3]MRC Centre for Inflammation Research, Queens Medical Research Institute, Edinburgh, United Kingdom. [4]The Beatson Institute for Cancer Research, Garscube Estate, Bearsden, Glasgow, United Kingdom. [5]Department of Molecular Biology, Vrije Universiteit, Amsterdam, Netherlands. [6]Oncology iMED, AstraZeneca, Alderley Park, Macclesfield, United Kingdom.

Cholangiocarcinoma (CC) is typically diagnosed at an advanced stage and is refractory to surgical intervention and chemotherapy. Despite a global increase in the incidence of CC, little progress has been made toward the development of treatments for this cancer. Here we utilized human tissue; CC cell xenografts; a p53-deficient transgenic mouse model; and a non-transgenic, chemically induced rat model of CC that accurately reflects both the inflammatory and regenerative background associated with human CC pathology. Using these systems, we determined that the WNT pathway is highly activated in CCs and that inflammatory macrophages are required to establish this WNT-high state in vivo. Moreover, depletion of macrophages or inhibition of WNT signaling with one of two small molecule WNT inhibitors in mouse and rat CC models markedly reduced CC proliferation and increased apoptosis, resulting in tumor regression. Together, these results demonstrate that enhanced WNT signaling is a characteristic of CC and suggest that targeting WNT signaling pathways has potential as a therapeutic strategy for CC.

Introduction

Great effort has been made to develop WNT inhibitors for cancer treatment; however, key questions remain unanswered, including which cancers depend on WNT signaling for their growth or remain WNT responsive following therapy. This reliance on WNT signaling is still unclear in many tumors, which is a reason why the route to clinic of WNT inhibitors is uncertain. Of all cancers, colorectal cancer is most well known to be initiated by WNT-activating mutations. These mutations per se lead to insensitivity to inhibitors targeting the WNT ligand or the receptors (1). This class of drugs, which includes inhibitors of porcupine in order to inhibit WNT secretion and LRP6 to block cell surface signaling, are the best-characterized WNT inhibitors (2). An increasingly diverse collection of small molecules against the WNT pathway are being trialed clinically (3). It is therefore imperative to define cancers that are driven by WNT signaling to evaluate whether WNT inhibitors offer a tenable therapeutic strategy for cancer treatment.

Cholangiocarcinoma (CC) typically presents at an advanced stage, and tumors can be multifocal in nature. Moreover, CC is surgically unamenable and non-responsive to chemotherapy, leading to a very poor prognosis, with a survival rate of less than 5% over 5 years (4). The global incidence of CC is increasing and accounts for 15% of primary liver cancers (5).

Recent sequencing studies have shown that a subset of fluke-associated intrahepatic CCs (ICCs) have mutations in *RNF43*, which could confer increased WNT signaling (6). Although *RNF43* mutations and alterations in *APC* and *CTNNB1* are absent in sporadic CC (7, 8), we hypothesized that sporadic CC may require activation of WNT signaling akin to that of fluke-associated CC and that, in the absence of mutations in *APC* or *CTNNB1*, may remain sensitive to ligand or receptor inhibitors.

In this study we demonstrate that CC is a WNT-high tumor and that this WNT-high state is maintained by inflammatory macrophages in the surrounding stroma. These inflammatory macrophages express WNT7B ligand in line with what has been described in other contexts (9–11). In xenografts of human CC cells, a transgenic murine line that develops CC (12), and also a well-validated, chemically induced rat model of CC (13–17) that reflects the progression of CC in humans, we find that depletion of macrophages or inhibition of the canonical WNT pathway results in reduced tumor burden. This strategy offers, for the first time to our knowledge, a small molecule approach to the treatment of CC in vivo. Furthermore, we demonstrate efficacy of these compounds in a non-transgenic model with a natural disease history, thereby identifying a tractable therapeutic for CC.

▶ Related Commentary: p. 975

Conflict of interest: The authors have declared that no conflict of interest exists.
Submitted: April 2, 2014; **Accepted:** December 18, 2014.
Reference information: *J Clin Invest*. 2015;125(3):1269–1285. doi:10.1172/JCI76452.

Results

The canonical WNT pathway is activated in human CC. The canonical WNT signaling pathway is upregulated in human CC when compared with patient-matched distal, non-cancerous liver (Figure 1A and Supplemental Tables 1 and 2; supplemental material available online with this article; doi:10.1172/JCI76452DS1). As well as multiple FZD receptors, the ligands *WNT7B* and *WNT10A* are highly overexpressed in CC (Supplemental Table 2), suggesting the WNT pathway may be important in CC progression and growth. Activity through the WNT signaling pathway was assayed

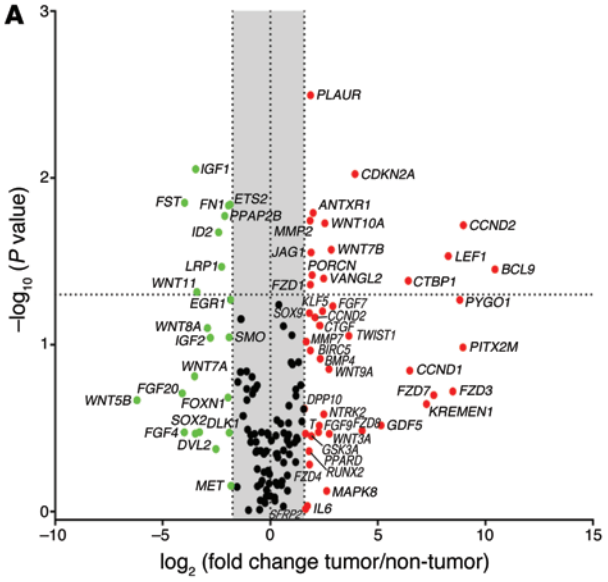
A
−log10 (P value)
log2 (fold change tumor/non-tumor)
PLAUR
CDKN2A
IGF1
FST
FN1
ETS2
PPAP2B
ANTXR1
WNT10A
CCND2
ID2
MMP2
JAG1
WNT7B
LEF1
BCL9
LRP1
PORCN
VANGL2
CTBP1
WNT11
FZD1
EGR1
KLF5
FGF7
CCND2
PYGO1
WNT8A
SOX9
CTGF
IGF2
SMO
MMP7
TWIST1
PITX2M
BIRC5
WNT7A
BMP4
WNT9A
CCND1
FGF20
FZD7
FZD3
WNT5B
FOXN1
DPP10
KREMEN1
SOX2
DLK1
NTRK2
FGF4
FGF9
FZD8
GDF5
DVL2
WNT3A
GSK3A
PPARD
FZD4
RUNX2
MET
MAPK8
IL6
SFRP2

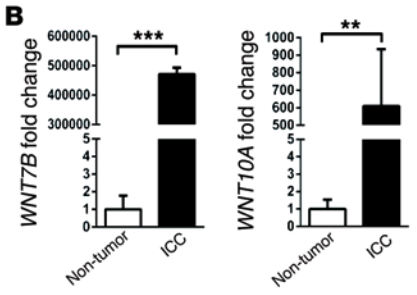
B
WNT7B fold change
WNT10A fold change
***
**
Non-tumor
ICC

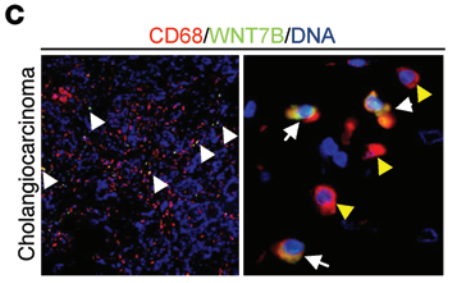
C
CD68/WNT7B/DNA
Cholangiocarcinoma

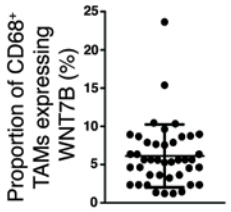
D
Proportion of CD68+ TAMs expressing WNT7B (%)

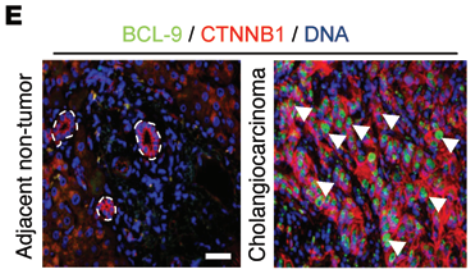
E
BCL-9 / CTNNB1 / DNA
Adjacent non-tumor
Cholangiocarcinoma

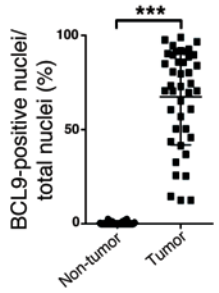
F
BCL9-positive nuclei/ total nuclei (%)
***
Non-tumor
Tumor

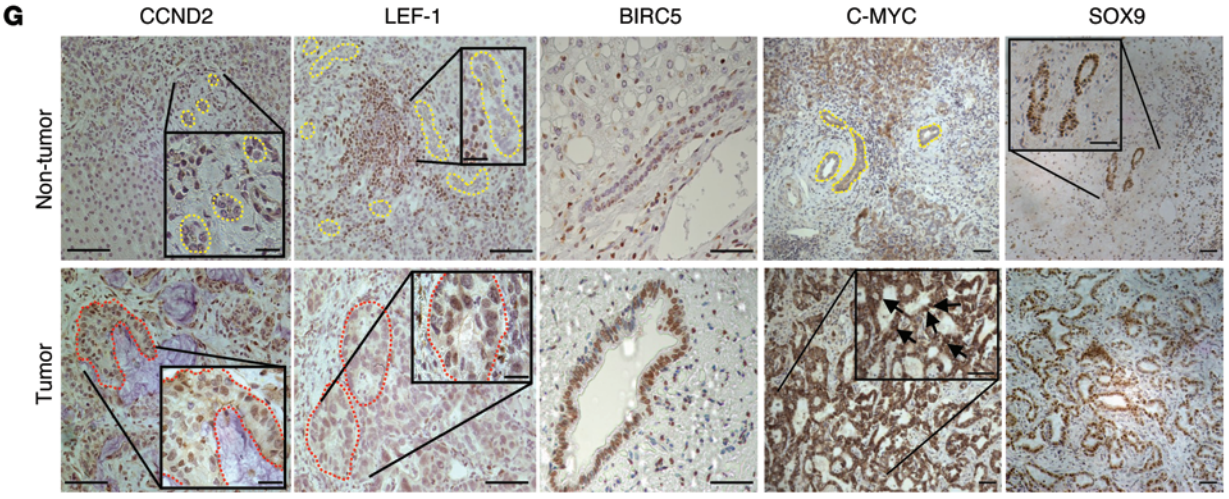
G
CCND2
LEF-1
BIRC5
C-MYC
SOX9
Non-tumor
Tumor

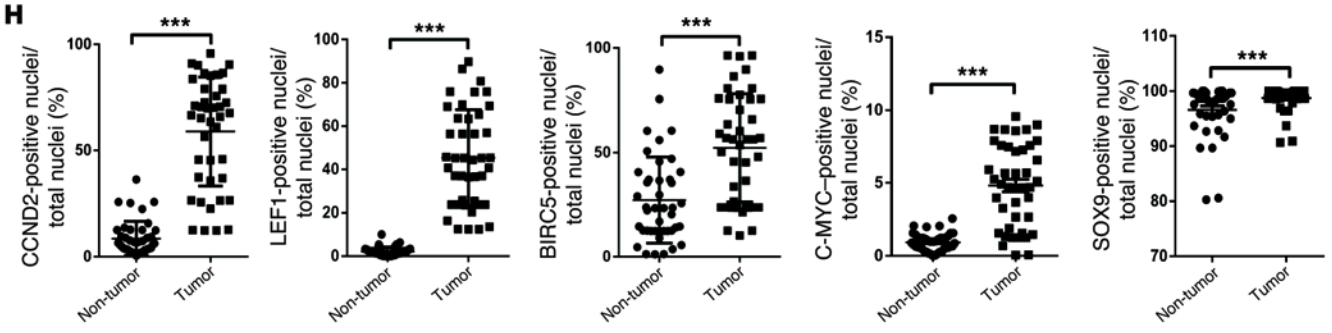
H
CCND2-positive nuclei/ total nuclei (%)
LEF1-positive nuclei/ total nuclei (%)
BIRC5-positive nuclei/ total nuclei (%)
C-MYC–positive nuclei/ total nuclei (%)
SOX9-positive nuclei/ total nuclei (%)
***
Non-tumor
Tumor

Figure 1. Canonical WNT signaling is activated in human CC. (**A**) mRNA expression of WNT pathway genes and WNT target genes in CC versus patient-matched non-cancerous tissue (n = 11). Represented as a 3-fold change; $P < 0.05$. (**B**) *WNT7B* and *WNT10A* mRNA expression in human CC versus non-diseased liver (n = 37 vs. n = 30). (**C**) Immunohistochemistry of WNT7B (green) in CD68-positive macrophages (red). (**D**) Quantification of $CD68^+WNT7B^+$ TAMs (n = 42). (**E**) Immunohistochemistry for CTNNB1 (red) and BCL9 (green) in human CC and non-tumor, patient-matched liver. (**F**) Quantification of biliary nuclear staining for BCL9 (n = 42 per group). (**G**) Immunohistochemistry in non-tumor versus CC for CCND2, LEF1, BIRC5, C-MYC, and SOX9. Yellow lines, non-cancerous bile ducts; red lines, malignant biliary ducts; black arrows, nuclear positivity for C-MYC. (**H**) Quantification of biliary nuclear staining for CCND2, LEF1, BIRC5, C-MYC, and SOX9 in non-tumor and CC tissue (n = 42 per group). Data are presented as mean ± SEM. Mann-Whitney U test; $^{**}P < 0.01$, $^{***}P < 0.001$. Photomicrograph scale bars: 50 μm (in **C**, right panel, 20 μm).

using 84 known CTNNB1 targets. In this matched cohort, we found upregulation of cell cycle genes including *CCND2*, *CDKN2A*, and *BIRC5*. Moreover, we found upregulation of multiple genes associated with a naive, undifferentiated state, including *JAG1*, *KLF5*, and *SOX9* (18–20), as well as genes involved in regulation of wound repair often deregulated in cancer: *PLAUR*, *MMP2*, and *MMP7* (21, 22) (Figure 1A and Supplemental Table 2). Interestingly, we also saw upregulation of *KREMEN1*, the non-obligate binding partner of the DKK family of WNT inhibitors (although we did not see upregulation of *DKK*). Recent data from zebrafish have implicated KREMEN1 in the restriction of DKK1 activity, thereby promoting WNT activity (23). Whether expression of KREMEN1 in human CC also promotes signaling is unclear. These data together indicate that there is an intact WNT signaling cascade that is overexpressed in human CC compared with matched patient non-cancerous liver.

Informed by our initial small, matched cohort, we looked at the expression of WNT7B and WNT10A in archival tissues from 37 pathologically confirmed CC cases (both intrahepatic and perihilar CC but no CC of the common bile duct; for complete clinical parameters, see Supplemental Table 1) versus 30 cases of healthy liver (from a sudden death brain bank (Supplemental Table 1). In non-cancerous liver, these WNT ligands were expressed at low but detectable levels, potentially reflecting an active WNT pathway in periportal zone 3 hepatocytes (24) or, indeed, WNT signaling on the background of disease. There was, however, significant overexpression of the *WNT7B* and *WNT10A* ligands in CC compared with non-cancerous controls (Figure 1B). We stained for the WNT10A and WNT7B proteins in human CC. While WNT10A was undetectable at the protein level in the liver (data not shown), we found expression of WNT7B throughout the CC stroma, frequently colocalizing with a subpopulation of $CD68^+$ macrophages (Figure 1C and Supplemental Figure 1A) and representing approximately 5% of the CD68-positive tumor-associated macrophages (TAMS) within the tumor stroma (Figure 1D).

To further confirm activation of the WNT pathway, we stained for CTNNB1, a core protein in the canonical WNT pathway. We could detect CTNNB1 in the membrane of human CC; however, we failed to detect the dephosphorylated form in the nucleus, likely due to its low stability in archival pathological specimens. We therefore stained human CC for an obligate binding partner of CTNNB1, BCL9 which is evolutionarily conserved and absolutely required for CTNNB1 to exert its canonical function (25–28). BCL9 was extensively expressed throughout the nuclei of the CC epithelium (Figure 1E and Supplemental Figure 1B), but not in the healthy bile ducts of non-cancerous matched tissue from 42 cases (0.38% in non-cancerous bile ducts vs. 67.44% in CC) (Figure 1F), confirming the importance of WNT pathway activation in human CC. We were able to stain human CC versus patient-matched non-tumor tissue (n = 42) for some of the canonical CTNNB1 targets we identified in our target array and found that an increased proportion of CC epithelial cells expressed the CTNNB1 targets CCND2 (12.58% vs. 63.52%), LEF1 (3.65% vs. 45.26%), BIRC5 (23.35% vs. 53.62%), C-MYC (0.93% vs. 4.80%), and SOX9 (95.56% vs. 98.73%) compared with non-cancerous biliary cells. (Figures 1, G and H, and Supplemental Figure 1B). These targets were largely expressed in the nucleus, as expected; however, C-MYC also demonstrated some strong cytoplasmic staining, which might represent recently described, non-transcriptional functions (29, 30).

The canonical WNT pathway is progressively activated during CC development. Because human CC tissue reflects end-stage disease, experiments using such samples do not address whether acquisition of a highly activated WNT pathway is a hallmark of CC development. To appropriately model CC development on the background of chronic damage, inflammation and repair, as seen in human disease, we used a model of chemically induced CC using thioacetamide (TAA). TAA induces chronic damage and regeneration, culminating in CC development after 26 weeks in both mouse and rat (Figure 2A, schematic, and Supplemental Figure 2B) that histologically and transcriptionally resembles that of the human cancer (13, 15, 16).

We have recently described a transgenic model of CC in which we specifically induce *p53* loss in keratin-19–expressing (KRT19-expressing) bile ducts using the tamoxifen-inducible *Krt19-CreER^T* transgenic line (12). Furthermore, recombined cells could be tracked through the presence of a silenced eYFP (Figure 2A, photomicrograph). Following tamoxifen induction and TAA administration, CC developed in *Krt19-CreER^T R26R-eYFP p53$^{fl/fl}$* mice, but not in *Krt19-CreER^T R26R-eYFP p53$^{fl/WT}$* or *Krt19-CreER^T R26R-eYFP p53$^{WT/WT}$* littermates. In *Krt19-CreER^T R26R-eYFP p53$^{fl/fl}$* mice, we found significant transcriptional upregulation of *Wnt7b* and *Wnt10a* compared with *Krt19-CreER^T R26R-eYFP p53$^{fl/WT}$* and *Krt19-CreER^T R26R-eYFP p53$^{WT/WT}$* mice (Figure 2B), suggesting that in these transgenic CCs, induced specifically with *p53* deletion, the WNT pathway becomes activated. We could observe two patterns of staining with WNT7B: large inflammatory cells scattered throughout the CC stroma as well as on the surface of the malignant epithelium, which could represent autonomous signaling from the epithelial cells, or ligand being received by these cells. These data indicate activation of the canonical WNT signaling pathway by the WNT7B ligand (Figure 2C, single channels, and Supplemental Figure 2A). We stained for total CTNNB1 in these mouse tumors and could detect staining in the membrane, but also strong staining in the cytoplasm and nucleus, indicating that in these biliary tumors the canonical WNT signaling pathway is active; however, we did not see nuclear and cytoplasmic staining in parenchymal hepatocytes or non-malignant ducts (Figure 2D and Supplemental Figure 2C). To confirm that the canonical WNT signaling pathway was indeed activated, we looked for expression

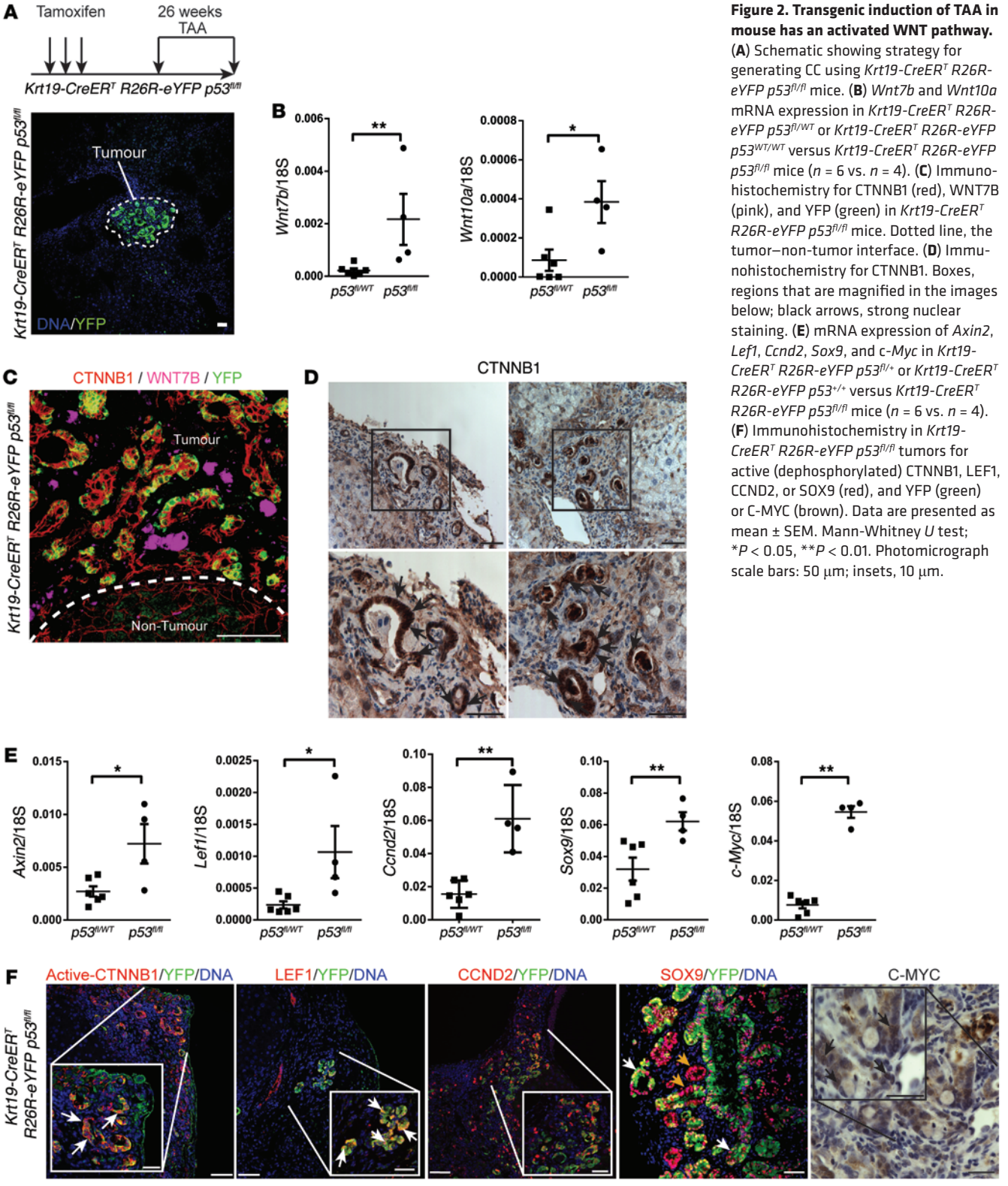

Figure 2. Transgenic induction of TAA in mouse has an activated WNT pathway. (**A**) Schematic showing strategy for generating CC using *Krt19-CreER^T R26R-eYFP p53$^{fl/fl}$* mice. (**B**) *Wnt7b* and *Wnt10a* mRNA expression in *Krt19-CreER^T R26R-eYFP p53$^{fl/WT}$* or *Krt19-CreER^T R26R-eYFP p53$^{WT/WT}$* versus *Krt19-CreER^T R26R-eYFP p53$^{fl/fl}$* mice (n = 6 vs. n = 4). (**C**) Immunohistochemistry for CTNNB1 (red), WNT7B (pink), and YFP (green) in *Krt19-CreER^T R26R-eYFP p53$^{fl/fl}$* mice. Dotted line, the tumor–non-tumor interface. (**D**) Immunohistochemistry for CTNNB1. Boxes, regions that are magnified in the images below; black arrows, strong nuclear staining. (**E**) mRNA expression of *Axin2*, *Lef1*, *Ccnd2*, *Sox9*, and c-*Myc* in *Krt19-CreER^T R26R-eYFP p53$^{fl/+}$* or *Krt19-CreER^T R26R-eYFP p53$^{+/+}$* versus *Krt19-CreER^T R26R-eYFP p53$^{fl/fl}$* mice (n = 6 vs. n = 4). (**F**) Immunohistochemistry in *Krt19-CreER^T R26R-eYFP p53$^{fl/fl}$* tumors for active (dephosphorylated) CTNNB1, LEF1, CCND2, or SOX9 (red), and YFP (green) or C-MYC (brown). Data are presented as mean ± SEM. Mann-Whitney *U* test; $^*P < 0.05$, $^{**}P < 0.01$. Photomicrograph scale bars: 50 μm; insets, 10 μm.

of the WNT targets *Axin2*, *Lef1*, *Ccnd2*, *Sox9*, and *c-Myc* and found that there was upregulated expression of these genes in *Krt19-CreER^T R26R-eYFP p53$^{fl/fl}$* but not *p53$^{fl/WT}$* or *p53$^{WT/WT}$* mice (Figure 2E). Moreover, we were able to detect dephosphorylated (nuclear) CTNNB1 (detecting an epitope distinct from that used in Figure 2D), nuclear LEF1, CCND2, SOX9, and C-MYC in the *p53$^{-/-}$* YFP$^+$ tumors (Figure 2F), indicating WNT signaling activity. We failed to see nuclear C-MYC staining in the nuclei of hepatocytes or non-malignant biliary epithelium (Supplemental Figure 2B).

Human *TRP53* (p53) is mutated in only a small proportion (9.3%) of spontaneous, non-liver fluke-associated CCs, indicating that a complex and heterogeneous group of mutations are capa-

ble of driving CC progression (31). Our murine model with Cre recombinase–induced p53 loss, therefore, is unlikely to represent the broad mutational profile seen in human CC. In order to assess experimentally how the WNT pathway regulates CC growth without prior genetic modification, we used TAA-induced carcinogenesis in rats as a more genetically appropriate model of CC.

Throughout the early stages of the rat TAA model of CC (up to 16 weeks), membranous CTNNB1 was detectable in the cell membrane of KRT19-positive regenerating ductules (Figure 3A and Supplemental Figure 2B). During CC formation (from week 20), we were able to detect high levels of dephosphorylated CTNNB1 in the nucleus of the epithelial component of CC (in 56% of epithelial cells) (Figure 3B and Figure 3E, graph). The canonical WNT pathway was highly activated in 26-week TAA-treated versus non-TAA age-matched controls. Upregulated targets included cell cycle regulators such as *Ccnd2*, *Cdkn2a*, and *Ctgf*, as well as targets associated with a progenitor phenotype, including *Jag1*, *Klf5*, and *Sox9*. These transcripts reflect a subset of genes that we found upregulated in human CC (Figure 1A), indicating that the TAA rat model mirrors the elevated WNT system we saw in humans (Figure 3C and Supplemental Table 3). Making use of our rat TAA time course, we were able to study the transcriptional changes of WNT pathway genes over time as the TAA model transitions from repair to carcinogenesis. The ligands *Wnt10a* and *Wnt7b* were both upregulated in the rat TAA model. *Wnt10a* transcription increased early, during the regenerative phase of this inflammatory model; however, *Wnt7b* increased in line with CC growth (Figure 3D). We also found that *Rspo1* expression was significantly upregulated in line with significant transcriptional induction of *Lgr4*, *Bcl9*, *Birc5*, *Axin2*, and *Rnf43*, the latter of which is an E3 ligase responsible for WNT-FZD receptor complex turnover. *RNF43* is mutated in a subset of fluke-associated CC in humans and results in a hyperactivated WNT signaling cascade (ref. 6 and Figure 3D). In addition to this, we found that aurora kinases A, B, and C (*Aurka*, *Aurkb*, and *Aurkc*) were expressed, with *Aurka* being highly upregulated during CC development, whereas *Aurkb* and *Aurkc* were increased but to a lesser degree throughout TAA treatment (Figure 3D). To confirm that the canonical WNT signaling pathway was indeed activated in the epithelial component of TAA-induced ICC, we stained samples from 26-week TAA-treated rats and found expression of BIRC5 in 84%, LEF1 in 63%, and CCND2 in 39% of cancerous epithelial cells (Figure 3E). As we believe WNT7B is important in human ICC (Figure 1A) and that its transcript expression increases in line with tumor growth in the TAA model, we sought to identify whether we could detect the WNT7B protein in ICC. In other regenerating systems, R-spondin is a coactivator of WNT signaling (32–35). We found a subset of the cancerous epithelium to which both RSPO-1 and WNT7B were bound (Figure 3F). Together, these data suggest that persistent activation of the WNT signaling pathway during chronic liver repair occurs in CC formation (36).

Macrophages are a source of WNT in CC. In human CC we found that CD68-positive macrophages were positive for WNT7B (Figure 1C). Similarly in TAA-induced CC in rat, CD68-positive macrophages expressed WNT7B protein in their cytoplasm. In addition to this we were able to detect WNT7B protein on a subset of cancerous epithelial cells in CC (Figure 4A), which may represent autonomous WNT signaling by the cancerous epithelium or demonstrate binding of the macrophage-derived ligand to the cell surface. We sought to ascertain whether the cells expressing WNT7B protein were derived from the BM, i.e., were inflammatory, or whether they were resident Kupffer cells, which are deposited embryonically from the yolk sac during hepatic organogenesis (37). We lethally irradiated wild-type rats and transplanted them with GFP-expressing BM, such that we could track cells in the liver that had originated from the adult hematopoietic system (Figure 4B). BM-transplanted rats given TAA developed CC in which a considerable proportion of the cancerous stroma was GFP expressing. In CC, $CD68^+$ TAMs were $CD163^-$ (therefore inflammatory) and GFP^+ (BM derived), and this population made up the bulk of the GFP-expressing cells in the tumor (Figure 4C). While very rare GFP^+CD163^+ cells could occasionally be seen at the tumor-parenchyma interface (Figure 4C), the $CD163^+$ population was predominantly GFP^- and not found within the tumor. We analyzed 10 independent TAA-induced rat tumors and found 96.7% of GFP^+CD68^+ TAMS also expressed CD206 (mannose receptor) (Figure 4, D and E), suggesting they are largely polarized to an alternatively activated, M2 phenotype (38). In TAA-induced tumors, approximately 19.93% of GFP^+CD68^+ macrophages expressed WNT7B at the protein level (Figure 4, F and G, and Supplemental Figure 2C), indicating that macrophages in the stroma of CC are of adult hematopoietic origin, not resident Kupffer cells, and that they represent the bulk of macrophage WNT7B expression in CC. We typically see two types of WNT7B staining in this context, granular staining throughout the cytoplasm of $CD68^+GFP^+$ cells and surface staining on the epithelium, potentially indicating a diverse origin of WNT7B in these tumors (Figure 4, A and F).

Loss of macrophage-derived WNT inhibits CC growth in vivo. To investigate whether macrophages play a functional role in CC growth in vivo, and whether this is a WNT-dependent phenomenon, we established a xenograft model of human CC. Three CC cell lines, CC-LP-1, SNU-1079, or WITT-1 cells (39, 40), were subcutaneously implanted in the flanks of CD1 nude mice. Within 21 days all mice had palpable tumors at the injection site. Xenografted mice were given liposomal clodronate (Lipclod) to selectively deplete phagocytic macrophages; GW2580 or AZD7507 (Figure 5A) to inhibit the activation of CSF receptor 1 (CSFR1), thereby preventing monocyte differentiation into macrophages; or appropriate vehicle alone (41–44). Tumors were isolated 8 hours after the final dose of each compound. The epithelial component of CC-LP-1, SNU-1079, or WITT-1 cells was negative for CSFR1; however, a population of small infiltrating cells expressed the receptor (Supplemental Figure 3A). In Lipclod-, GW2580-, and AZD7507-treated mice, we observed a significant decrease the number of $CD68^+$ macrophages in the xenografts (Figure 5B and Supplemental Figure 3B). Mice with CC-LP-1 and SNU-1079, but not WITT-1, xenografts demonstrated both reduced tumor volume and mass after treatment with Lipclod, GW2580, and AZD7507 (Figure 5C and Supplemental Figure 3C). Furthermore, of the 8 SNU-1079 xenografts that were palpable at 3 weeks, only 4 from the GW2580 group and 6 from the AZD7507 group were large enough to recover at week 6, as they were no longer palpable and too small to detect. In the CC-LP-1 group, only 3 of the 8 tumors were detectable at 6 weeks. (In the WITT-1 line, 7 xenografts were recovered from the GW2580 and 8 from the AZD7507 group.) Depletion of mac-

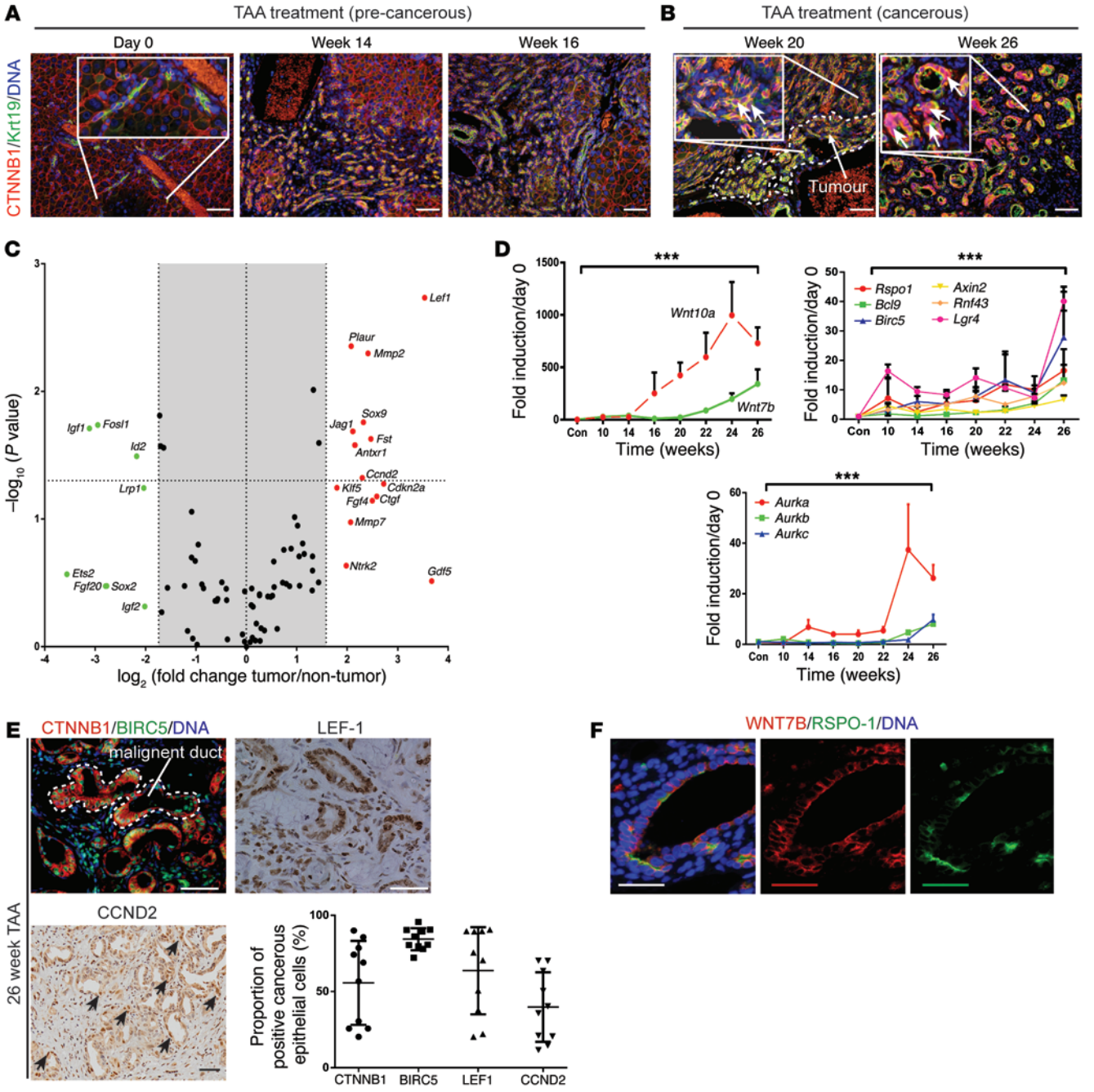

Figure 3. The WNT pathway is activated in a rat model of CC. (**A**) Immunohistochemistry for CTNNB1 (red) and KRT19 (green) in precancerous TAA rats. (**B**) Immunohistochemistry for CTNNB1 and KRT19 in cancerous TAA rats. White arrows in insets, nuclear positivity of CTNNB1; dotted line, tumor interface. (**C**) mRNA expression of WNT pathway targets in 26-week TAA versus matched non-treated controls (n = 6 per group). (**D**) mRNA expression of WNT ligands *Wnt10a* and *Wnt7b*; WNT pathway effectors *Rspo1*, *Bcl9*, *Birc5*, *Axin2*, *Rnf43*, and *Lgr4*; and cell cycle targets *Aurka*, *Aurkb*, and *Aurkc*. (**E**) Immunohistochemistry in rat CC for CTNNB1 (red), BIRC5 (green), and LEF1 and CCND2 (brown). Graph: Quantification of epithelial nuclear staining in 26-week TAA rat (n = 10). (**F**) Immunohistochemistry for WNT7B (red) and RSPO-1 (green) in TAA-induced CC. Data are presented as mean ± SEM. Kruskal-Wallis test; ***$P < 0.001$. Photomicrograph scale bars: 50 μm; insets, 10 μm.

rophages using Lipclod, GW2580, or AZD7507 in all 3 xenografted lines resulted in a reduction in murine *Wnt7b* expression at the mRNA level (Figure 5D and Supplemental Figure 3D). Murine and human WNT7B share 99% peptide similarity; therefore, we expected murine WNT7B would be sufficient to activate normal canonical WNT signaling in human CC lines. Concurrent with the loss of macrophages and host macrophage-derived murine *Wnt7b* expression, we found reduced expression of the human pro-proliferation genes *BIRC5*, *CCND2*, and *CCNE* (Supplemental Figure 3, E and H) and an increase in expression of *BAX1* in CC-LP-1 and SNU-1079 but not WITT-1 xenografts (Supplemental Figure 3, G and J), indicating ablation of macrophages and by extension loss of WNT signal, reduced proliferation, and induced apoptosis, thereby reducing tumor burden in CC-LP-1 and SNU-1079

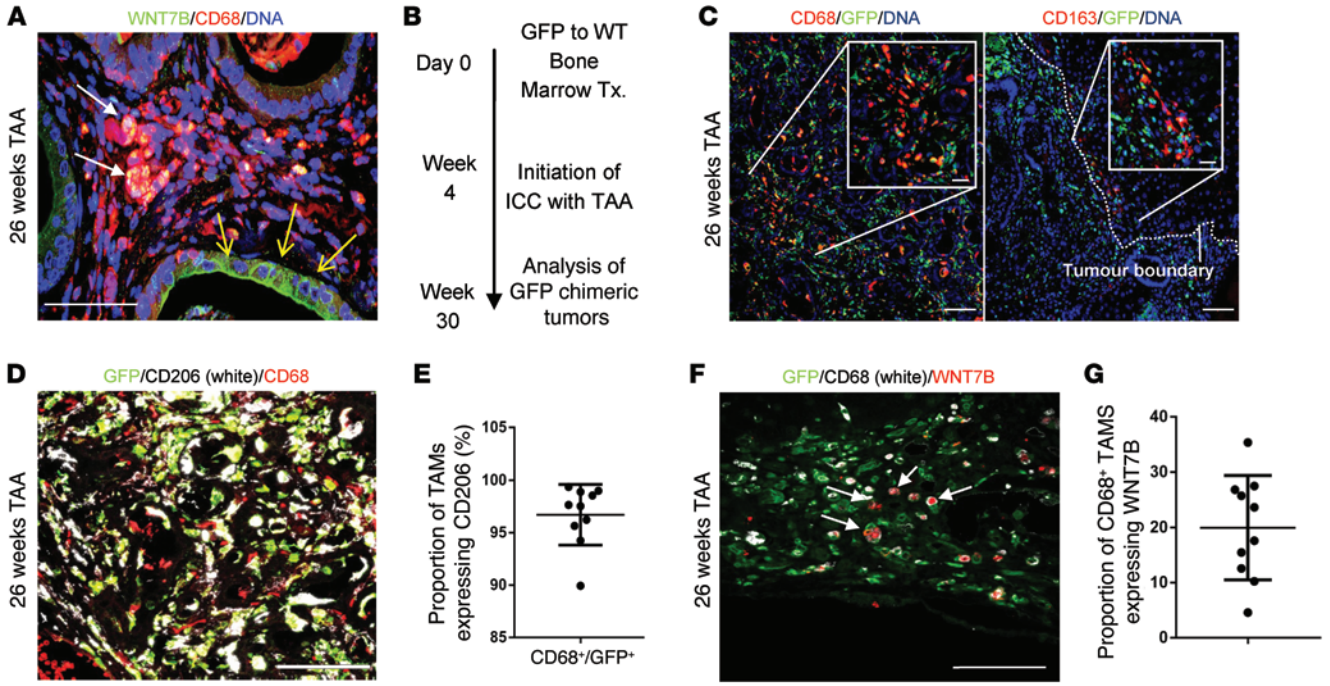

Figure 4. M2 macrophages initiate a WNT-high state in CC. (**A**) Immunohistochemistry in TAA-induced CC for WNT7B (green) and CD68 (red). White arrows, macrophage expression of WNT7B; yellow arrows, epithelial positivity for WNT7B. (**B**) Schematic representing the GFP BM transplant (Tx.) strategy. (**C**) Immunohistochemistry for CD68 or CD163 (red) and GFP (green) in 26-week TAA BM-transplanted rats. Dotted line, tumor boundary. (**D**) Immunohistochemistry of GFP (green)/CD68 (red) dual-positive TAMs expressing CD206 (white). (**E**) Quantification of CD68/GFP dual-positive TAMs expressing CD206 (n = 10). (**F**) Immunohistochemistry for GFP (green), CD68 (white), and WNT7B (red) in 26-week TAA CC. (**G**) Quantification of CD68-positive macrophages expressing WNT7B in rat CC (n = 10). Data are presented as mean ± SEM. Photomicrograph scale bars: 50 μm; insets, 10 μm.

xenografts in vivo. We confirmed this observation by staining for Ki-67 and TUNEL to look for proliferation and cell death, respectively, in our xenografts. We found an obvious reduction in Ki-67 positivity (photomicrographs, Supplemental Figure 3, F and I) and an increase in TUNEL positivity (photomicrographs, Supplemental Figure 3, G and J) in macrophage-depleted CC-LP-1 and SNU-1079 but not WITT-1 xenografts. The inconsistency seen in the WITT-1 group could reflect the extrahepatic origin of the WITT-1 line (45), which suggests it has a growth kinetic very different from the intrahepatic lines; that fact that it is less reliant on macrophage activation; or, alternatively, that it undergoes proliferative compensation from a signal that is non–macrophage derived.

Subcutaneous xenografts do not represent CC in terms of natural disease progression or stromal microenvironment. Therefore, we used our TAA-induced rat model of CC to ask whether macrophage ablation in CC alters canonical WNT pathway activity and whether this regulates in situ growth of CC (Figure 6A). Following administration of liposomal clodronate, both $CD68^+$ (inflammatory) and $CD163^+$ (resident) macrophages were significantly reduced in number (Supplemental Figure 4A). In line with this loss of macrophages, we found a significant reduction in the expression of *Wnt7b* and also a non-significant reduction in the M-BOAT family member porcupine (*Porcn*), which is necessary for WNT ligand secretion (46), but not *Wnt10a*, indicating that this ligand is not derived from macrophages in this model of CC (Figure 6B). We immunostained TAA tumor treated with Lipclod versus vehicle for WNT7B. In vehicle-treated animals, we could detect the presence of WNT7B on the cancerous duct (Figure 6C). Following macrophage depletion, however, we were unable to detect WNT7B protein on these malignant ducts (Figure 6C). We further analyzed activation of the WNT pathway by looking at CTNNB1 targets in tissue containing CC from macrophage-depleted versus control groups. Macrophage-depleted CC showed a global downregulation of CTNNB1 targets in vivo. We found significant downregulation of genes known to regulate cell cycle, including *Ccnd1*, *Ctgf*, and Hedgehog receptors *Ptch1* and *Smo*. Moreover, we found significant downregulation of genes known to promote a progenitor phenotype, including *Jag1* and *Klf5* (Figure 6D and Supplemental Table 3). The net consequence of macrophage depletion and WNT pathway inactivation in CC was a striking 86% reduction in tumor number and 90% reduction in tumor volume (Figure 6, E and F). To confirm that macrophage ablation was preventing activation of the canonical WNT pathway, we stained remaining CC rudiments and control CCs for nuclear CTNNB1 and BIRC5. We found CTNNB1 was confined to the cell membrane in cancer following macrophage ablation (Supplemental Figure 4B) and that it did not translocate to the nucleus as in the control tissue. BIRC5 was largely lost in the epithelial compartment of the tumor following macrophage depletion compared with control (73.17% in control vs. 25.56% in Lipclod treated, Supplemental Figure 4C). Expression of BIRC5 persisted in non-epithelial components of the tumor, indicating that macrophage depletion targets WNT activity in the epithelial compartment, whereas expression of BIRC5 is regulated in a non-WNT-dependent manner in the stroma. We also investigated the expression of known CTNNB1 targets SOX9, LEF1, and CCND2 in TAA-induced CCs treated with Lipclod versus vehicle.

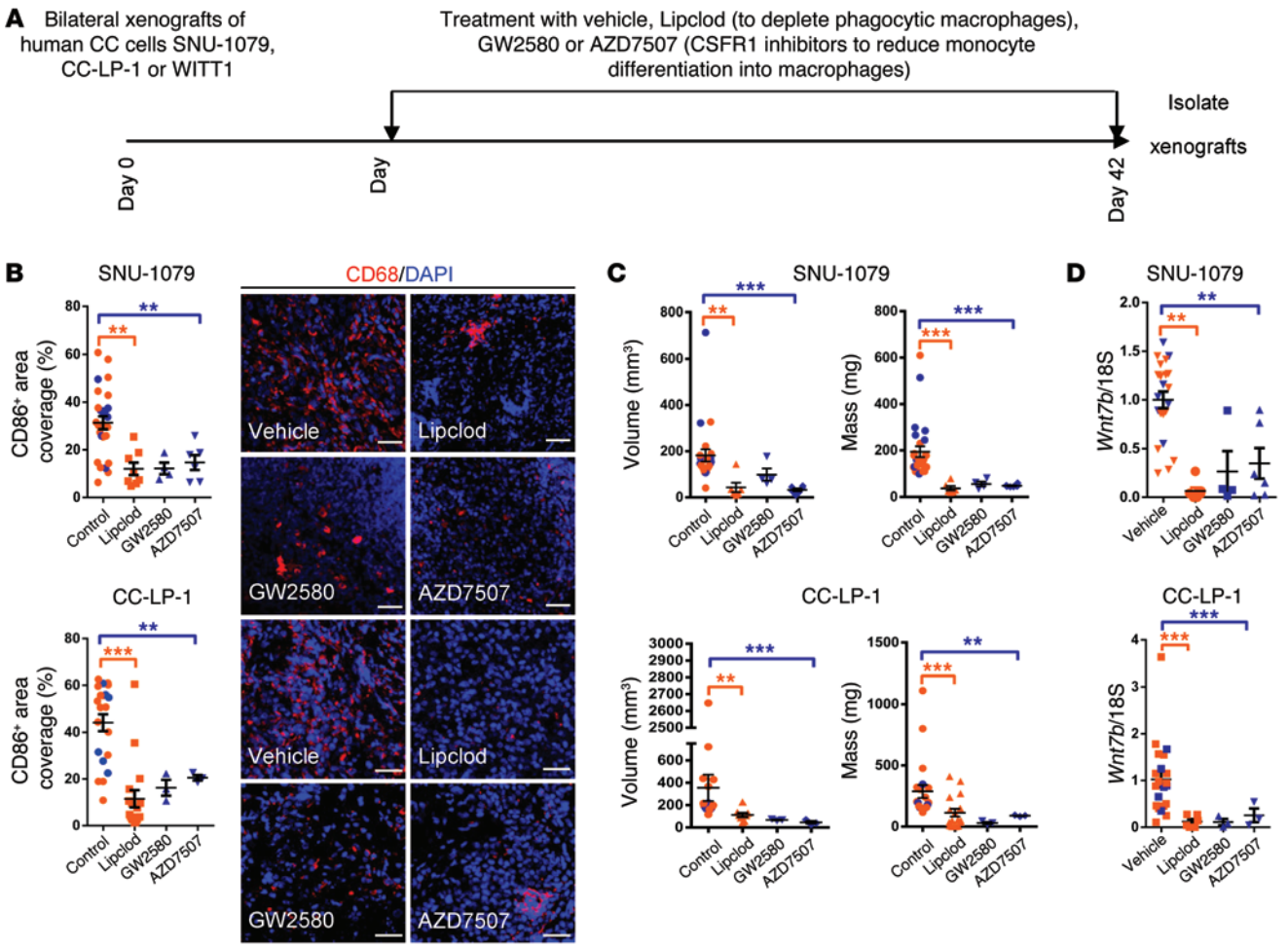

Figure 5. Macrophage ablation in human CC cell xenografts reduces tumor penetrance. (**A**) Schematic demonstrating the strategy for macrophage depletion in human CC cell xenografts. (**B**) Quantification of CD68-positive macrophage number in SNU-1079 and CC-LP-1 xenografts following treatment with Lipclod, GW2580, or AZD7507 compared with vehicle alone. Photomicrographs: Immunohistochemistry in xenografts for CD68-positive macrophages (red). (**C**) Volume and mass of SNU-1079 and CC-LP-1 xenografts following treatment with Lipclod, GW2580, or AZD7507 compared with vehicle alone. (**D**) Murine *Wnt7b* expression in SNU-1079 and CC-LP-1 xenografts following treatment with Lipclod, GW2580, or AZD7507 compared with vehicle alone. Data are presented as mean ± SEM. A Kruskal-Wallis test was used to compare GW2580 and AZD7507 and control. Lipclod and control were compared using a Mann-Whitney *U* test in both cases. $^{**}P < 0.01$, $^{***}P < 0.001$. Photomicrograph scale bars: 50 μm. For SNU-1079: PBS $n = 11$, liposomes $n = 8$, Lipclod $n = 8$, gavage vehicle $n = 8$, GW2580 $n = 4$, and AZD7507 $n = 6$. For CC-LP-1: PBS $n = 9$, liposomes $n = 6$, Lipclod $n = 15$, gavage vehicle $n = 6$, GW2580 $n = 3$, and AZD7507 $n = 3$.

We found a significant reduction in the epithelial nuclear positivity of SOX9 (96.05% in control vs. 75.54% in Lipclod treated, Supplemental Figure 4D), LEF1 (69.14% in control vs. 65.30% in Lipclod treated, Supplemental Figure 4E), and CCND2 (30.40% in control vs. 13.16% in Lipclod treated, Supplemental Figure 4F). In vehicle-treated animals, Ki-67 was readily detected in the malignant CC epithelium (in 52.9% of CC epithelia); however, TUNEL positivity was rare (in 2.7% of CC epithelia) (Supplemental Figure 4G). Upon macrophage depletion we detected notable regions ranging from groups of cells to entire ductules of the biliary epithelium that stained positive for TUNEL (18.17% positive). Moreover, we found a significant drop in the number of CC epithelial cells that were positive for Ki-67 (28.14%), indicating that reduction in tumor load is in part mediated through the induction of apoptosis and loss of proliferation in vivo (Supplemental Figure 4G).

CTNNB1 inhibition regulates cell cycle progression in CC. Systemic depletion of macrophages is not a tenable therapy for the treatment of CC; therefore, we sought to interrogate the WNT-CTNNB1 pathway in CC directly. In our PCR arrays of human CC, we found that both *CTBP1* and *PORCN* were highly upregulated (Figure 1A). CTNNB1-CTBP activates transcription of pro-proliferative WNT target genes (47), whereas PORCN is required for the palmitoylation of WNT ligands, thereby regulating their secretion (48, 49). Thus, we specifically inhibited either the CTNNB1-CTBP interaction or the activity of PORCN in human CC cells in vitro with the small molecule ICG-001 or C-59, respectively. These compounds have been used to great effect in other systems (47, 50–53) to therapeutically inhibit the canonical WNT signaling cascade. Five human CC cell lines, CC-LP-1, SNU-1079, WITT-1, SNU-1196, and CC-SW-1 (39, 40, 54), expressed both CTNNB1 and WNT7B in vitro (Supplemental Figure 5A; negative staining control, Supplemental Figure 8B). Inhibition of CTNNB1-CTBP or PORCN with ICG-001 or C-59, respectively, resulted in a reduction in cell number in a dose-dependent manner (Figure 7A) across all

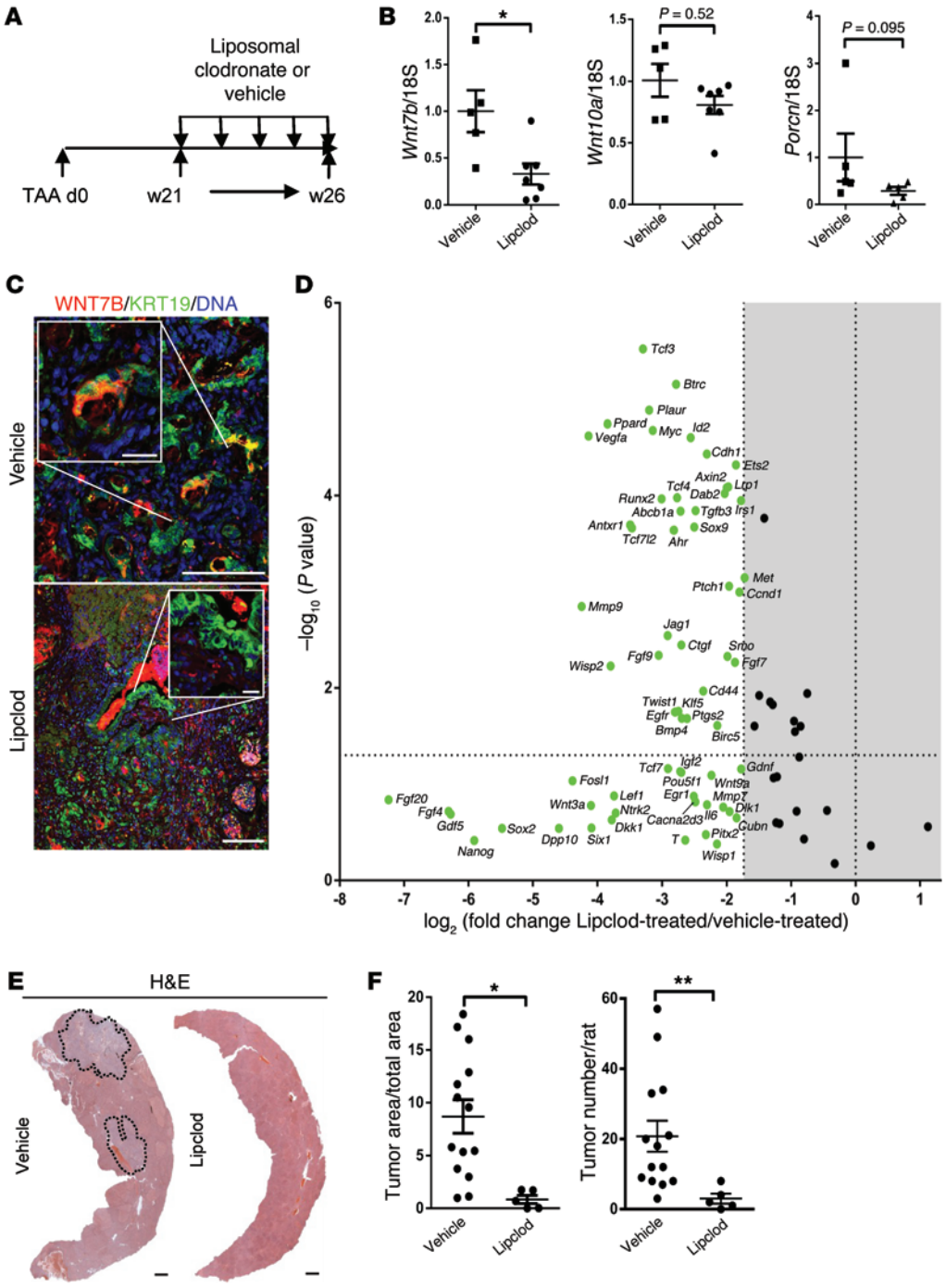

Figure 6. Macrophage inhibition reduces CC growth in vivo. (**A**) Schematic representing macrophage depletion in TAA using Lipclod. (**B**) mRNA expression of *Wnt7b*, *Wnt10a*, and *Porcn* following macrophage depletion in TAA CC using vehicle versus Lipclod (n = 5 vs. n = 7). (**C**) Immunohistochemistry on vehicle- versus Lipclod-treated TAA tissue for WNT7B (red) and KRT19 (green). (**D**) mRNA expression of WNT pathway target genes following Lipclod depletion of macrophages (n = 6 per group); green denotes downregulation. Represented as a 3-fold change; $P < 0.05$ (**E**) H&E of rat liver from TAA rats treated with vehicle versus Lipclod. (**F**) Quantification of area and number of rat TAA-induced CC tumors following treatment with vehicle or Lipclod (n = 14 vs. n = 5). Data are represented as mean ± SEM. Mann-Whitney U test; $^*P < 0.05$, $^{**}P < 0.01$. Scale bars in **C**: 50 μm; insets, 10 μm. Scale bars in **E**: 1 mm.

5 lines. Reduction in the viability of cells treated with either ICG-001 or C-59 was due to both reduced proliferation of CC cells and increased apoptosis, as demonstrated by reduced BrdU uptake and increased caspase-3/7 activity in CC cells (Figure 7, B and C). Inhibition of the canonical WNT signaling pathway using both small molecule strategies reduced the expression of numerous WNT target genes in all cell lines tested (Figure 7, D and E, Supplemental Figure 6, A and B, and Supplemental Table 4). There was no stereotypical group of targets that was downregulated in CC lines following ICG-001 or C-59 treatment; this may reflect the diverse origins of these CC lines or highlight how canonical WNT signaling promotes survival through multiple pathways. To ascertain how inhibition of canonical WNT signaling was exerting its effect to reduce CC cell numbers, we assessed cell cycle genes that were diversely regulated in ICG-001– or C-59–treated versus vehicle-treated cells (Figure 7, D and E, Supplemental Figure 6, A and B, and Supplemental Table 4). In both ICG-001– and C-59–treated CC lines, we saw downregulation of multiple genes that govern multiple phases of the cell cycle, suggesting that in vitro reduction in CC cell number is due to global repression of proliferation.

To test whether ICG-001 and C-59 is efficacious in reducing CC growth in vivo, we xenografted 3 CC cell lines (WITT-1, CC-LP-1, and CC-SW-1) into the flanks of CD1 nude mice and treated them with ICG-001, C-59, or vehicle alone. In the

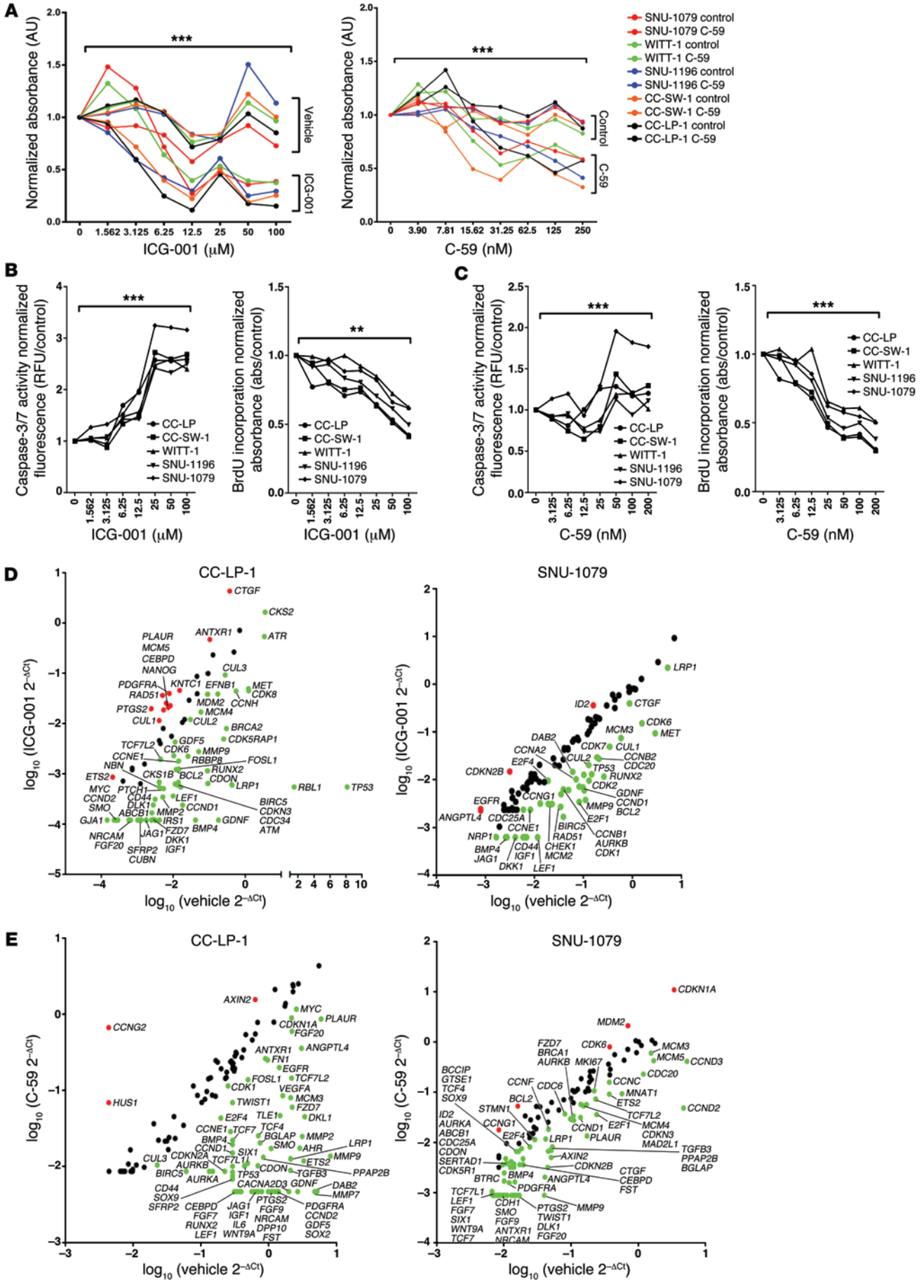
A
Normalized absorbance (AU)
***
Vehicle
ICG-001
ICG-001 (μM)
0 1.562 3.125 6.25 12.5 25 50 100
Control
C-59
C-59 (nM)
0 3.90 7.81 15.62 31.25 62.5 125 250
SNU-1079 control
SNU-1079 C-59
WITT-1 control
WITT-1 C-59
SNU-1196 control
SNU-1196 C-59
CC-SW-1 control
CC-SW-1 C-59
CC-LP-1 control
CC-LP-1 C-59
B
Caspase-3/7 activity normalized fluorescence (RFU/control)
BrdU incorporation normalized absorbance (abs/control)
**
CC-LP
CC-SW-1
WITT-1
SNU-1196
SNU-1079
C
D
CC-LP-1
SNU-1079
log10 (ICG-001 2−ΔCt)
log10 (vehicle 2−ΔCt)
CTGF CKS2 ANTXR1 ATR PLAUR MCM5 CEBPD NANOG CUL3 PDGFRA KNTC1 EFNB1 MET RAD51 CDK8 MDM2 CCNH PTGS2 MCM4 CUL1 CUL2 BRCA2 GDF5 CDK5RAP1 TCF7L2 CDK6 MMP9 CCNE1 RBBP8 FOSL1 NBN RUNX2 CKS1B BCL2 CDON ETS2 LRP1 RBL1 TP53 MYC PTCH1 CCND2 CD44 LEF1 BIRC5 SMO DLK1 CCND1 CDKN3 ABCB1 MMP2 CDC34 GJA1 IRS1 GDNF ATM JAG1 FZD7 BMP4 NRCAM DKK1 FGF20 SFRP2 IGF1 CUBN
ID2 CTGF LRP1 CDK6 MCM3 MET DAB2 CDK7 CUL1 CCNA2 CUL2 CCNB2 E2F4 TP53 CDC20 CDKN2B RUNX2 CDK2 GDNF EGFR CCNG1 MMP9 CCND1 BCL2 ANGPTL4 CDC25A E2F1 CCNE1 BIRC5 NRP1 RAD51 CCNB1 BMP4 CD44 CHEK1 AURKB JAG1 IGF1 MCM2 CDK1 DKK1 LEF1
E
log10 (C-59 2−ΔCt)
log10 (vehicle 2−ΔCt)
AXIN2 MYC CCNG2 CDKN1A PLAUR FGF20 ANTXR1 ANGPTL4 FN1 EGFR FOSL1 TCF7L2 CDK1 VEGFA HUS1 TWIST1 MCM3 FZD7 E2F4 TLE1 DKL1 CCNE1 TCF7 TCF4 BMP4 BGLAP LRP1 CCND1 SMO AHR SIX1 CUL3 CDKN2A MMP9 TCF7L1 ETS2 AURKB CDON TGFB3 PPAP2B BIRC5 TP53 AURKA CACNA2D3 GDNF DAB2 CD44 MMP7 SOX9 PTGS2 PDGFRA SFRP2 CEBPD JAG1 FGF9 CCND2 FGF7 IGF1 NRCAM GDF5 RUNX2 IL6 DPP10 SOX2 LEF1 WNT9A FST
CDKN1A MDM2 FZD7 CDK6 MCM3 BRCA1 MCM5 CCND3 AURKB MKI67 CDC20 BCCIP CCNF CDC6 CCNC GTSE1 MNAT1 TCF4 BCL2 CCND2 SOX9 STMN1 ETS2 ID2 TCF7L2 AURKA CCNG1 CCND1 E2F1 MCM4 ABCB1 E2F4 LRP1 PLAUR CDKN3 CDC25A MAD2L1 CDON AXIN2 TGFB3 SERTAD1 CDKN2B PPAP2B CDK5R1 CTGF BGLAP BTRC BMP4 ANGPTL4 CEBPD PDGFRA FST TCF7L1 LEF1 CDH1 PTGS2 MMP9 FGF7 SMO TWIST1 SIX1 FGF9 DLK1 WNT9A ANTXR1 FGF20 TCF7 NRCAM

Figure 7. Inhibition of the canonical WNT signaling pathway alters cell viability in vitro. (**A**) MTT assay using SNU-1079, CC-SW-1, SNU-1196, CC-LP-1, and WITT-1 CC lines treated with increasing concentrations of ICG-001 or C-59. Dose response data are presented as the mean of 3 experimental replicates that were run in triplicate. (**B**) Quantification of caspase-3/7 activity and BrdU incorporation with increasing concentrations of ICG-001 in SNU-1079, CC-SW-1, SNU-1196, CC-LP-1, and WITT-1 CC lines. (**C**) Quantification of caspase-3/7 activity (left graph) and BrdU incorporation (right graph) with increasing concentrations of C-59 in SNU-1079, CC-SW-1, SNU-1196, CC-LP-1, and WITT-1 CC lines. (**D**) mRNA expression of WNT target genes and cell cycle genes in CC-LP-1 and SNU-1079 cells following inhibition with ICG-001. Data are presented as >2-fold-change. (**E**) mRNA expression of WNT target genes and cell cycle genes in CC-LP-1 and SNU-1079 cells following inhibition with C-59. Data are presented >2-fold-change. Dose response data are presented as the mean of 3 experimental replicates that were run in triplicate. Kruskal-Wallis test; $^{**}P < 0.01$, $^{***}P < 0.001$. Gene expression data represent pooled material from 3 experimental replicates run in triplicate.

xenografted extrahepatic CC cell line WITT-1, there was again no statistically significant difference in either the mass or volume of the xenografts following WNT signaling inhibition (Supplemental Figure 6C). The mass and volume of CC-LP-1 and SNU-1079 xenografts were reduced in both the ICG-001– and C-59–treated groups compared with vehicle (Supplemental Figure 6, G and K). Curiously, we found a moderate reduction in mouse *Wnt7b* mRNA expression in both ICG-001– and C-59–treated xenografts, indicating WNT7B could itself be a target of the WNT-CTNNB1 signaling pathway (Supplemental Figure 6, D, H, and L). In line with this, we observed reduced proliferation in CC-LP-1 and SNU-1079, but not WITT-1, CC xenografts, as demonstrated by a reduction in the human cell cycle genes *BIRC5*, *CCND2*, and *CCNE* (Supplemental Figure 6, E, I, and M). Concurrently we found an increase in apoptosis reflected in expression of human *BAX1* within the CC-LP-1 and SNU-1079, but not WITT-1, CC xenografts (Supplemental Figure 6, F, J, and N).

Inhibition of canonical WNT signaling inhibits CC growth. Our data demonstrate that the WNT signaling pathway is required for proliferation and survival of CC in xenografts. To confirm that these findings are translatable into a pathophysiological model of CC in vivo, we gave the CTNNB1-CTBP inhibitor ICG-001 to rats treated with TAA for 26 weeks. Furthermore, as we hypothesize that CC is still dependent on WNT ligand due to relatively infrequent mutations in *Apc* or *Ctnnb1*, we inhibited WNT ligand secretion using the small molecule C-59, as this compound also inhibited human CC growth in vitro and in xenografts (2, 53, 55, 56). We administered ICG-001, C-59, or vehicle alone once tumors had established at week 21, through to week 26, during which tumors normally undergo rapid growth (Figure 8A). Inhibition of the canonical WNT pathway with either ICG-001 or C-59 resulted in a marked decrease in tumor burden throughout the liver lobe (Figure 8B). Reduced tumor penetrance was largely due to a decrease in tumor number in both ICG-001– and C-59–treated animals compared with vehicle alone (76% and 64% reduction respectively) (Figure 8, B and C). Moreover, the size of the remaining tumors was significantly reduced by 71% in the ICG-001–treated group and 78% in the C-59–treated animals (Figure 8, B and C). Inhibition of WNT ligand secretion with C-59 or inhibition of CTNNB1-CTBP by ICG-001 resulted in large-scale downregulation of WNT target genes in CC-containing tissue from inhibited versus control CCs. Many of the genes that were significantly downregulated in these CCs were associated with growth factor signaling, including *Fgf7* and *Fgf9*, or genes typically associated with progenitor maintenance, including *Jag1* and *Klf5* (Figure 8, D and E, volcano plots, and Supplemental Table 5). We found *Ccne* and *Ccnd2* were consistently and significantly downregulated following WNT pathway inhibition. The two independent WNT pathway inhibitors ICG-001 and C-59 did not modulate distinct targets of the canonical WNT pathway (Figure 8F). Earlier generations of WNT signaling inhibitors could not be used therapeutically, as they had significant off-target, systemic effects (3). In this study neither ICG-001– nor C-59–treated animals demonstrated any additional symptoms aside from chronic disease induced by TAA. Weight monitoring and body condition were evaluated during these studies, and no discernible differences were detected throughout (Supplemental Figure 7A). At the end of treatment, blood serum was taken from all animals. There was no significant difference in serum alkaline phosphatase (ALP), bilirubin, aspartate transaminase (AST), alanine transaminase (ALT), or albumin (Supplemental Figure 7B), indicating that WNT inhibition modulates tumor growth but does not affect the severity of underlying disease.

In the cancerous biliary epithelium of rats given TAA followed by vehicle alone, both BIRC5 and dephosphorylated CTNNB1 proteins were found in the nuclei of the epithelial compartment of the tumor (Figure 9, A and B). Inhibition with C-59 greatly reduced the nuclear positivity of CTNNB1 in the cancerous epithelium (71.91% vs. 3.501%). BIRC5 was also reduced in the epithelial compartment (67.83% vs. 20.62%) (Figure 9, C and D); however, strong staining for BIRC5 in non-epithelial cell types in the CC stroma could still be observed, indicating non-epithelial expression of BIRC5 is independent of the WNT signal (Figure 9C). ICG-001 did not completely inhibit the translocation of CTNNB1 to the nucleus in CC (Figure 9A, 71.91% vs. 28.90%); however, this inhibitor elicits its effect downstream of nuclear translocation of CTNNB1. In ICG-001–treated CC, we found the CTNNB1-CTBP target BIRC5 was almost completely lost in the epithelium of CC treated with ICG-001 (Figure 9, B and C, 67.83% vs. 18.63%), again demonstrating that inhibition of the WNT signaling cascade was sufficient to inhibit CTNNB1 target expression.

In C-59– or ICG-001–treated rats, the remaining cancerous epithelia still had regions of proliferation, potentially reflecting a population of WNT inhibitor–resistant cancer cells (vehicle 63.78%, ICG-001 49.67%, and C-59 49.73% Ki-67$^+$ CC epithelial cells); however, there were also large regions of TUNEL positivity in the cancerous epithelium (vehicle 0.86%, ICG-001 6.529%, and C-59 4.551% TUNEL$^+$ CC epithelia), suggesting that in the absence of active WNT signaling, tumors were unable to maintain growth and underwent apoptosis (Figure 9, E and F). Moreover, in these inhibitor-treated rats we saw a downregulation of the known WNT-regulated cell cycle genes *Aurka* and *Aurkb* (Supplemental Figure 7C), suggesting that in the TAA rat model of CC, WNT-dependent cell cycle progression is important for the proliferation of the tumor.

Discussion

One of the archetypal functions of the canonical WNT signal is to drive cell proliferation in a variety of cell types. It achieves this

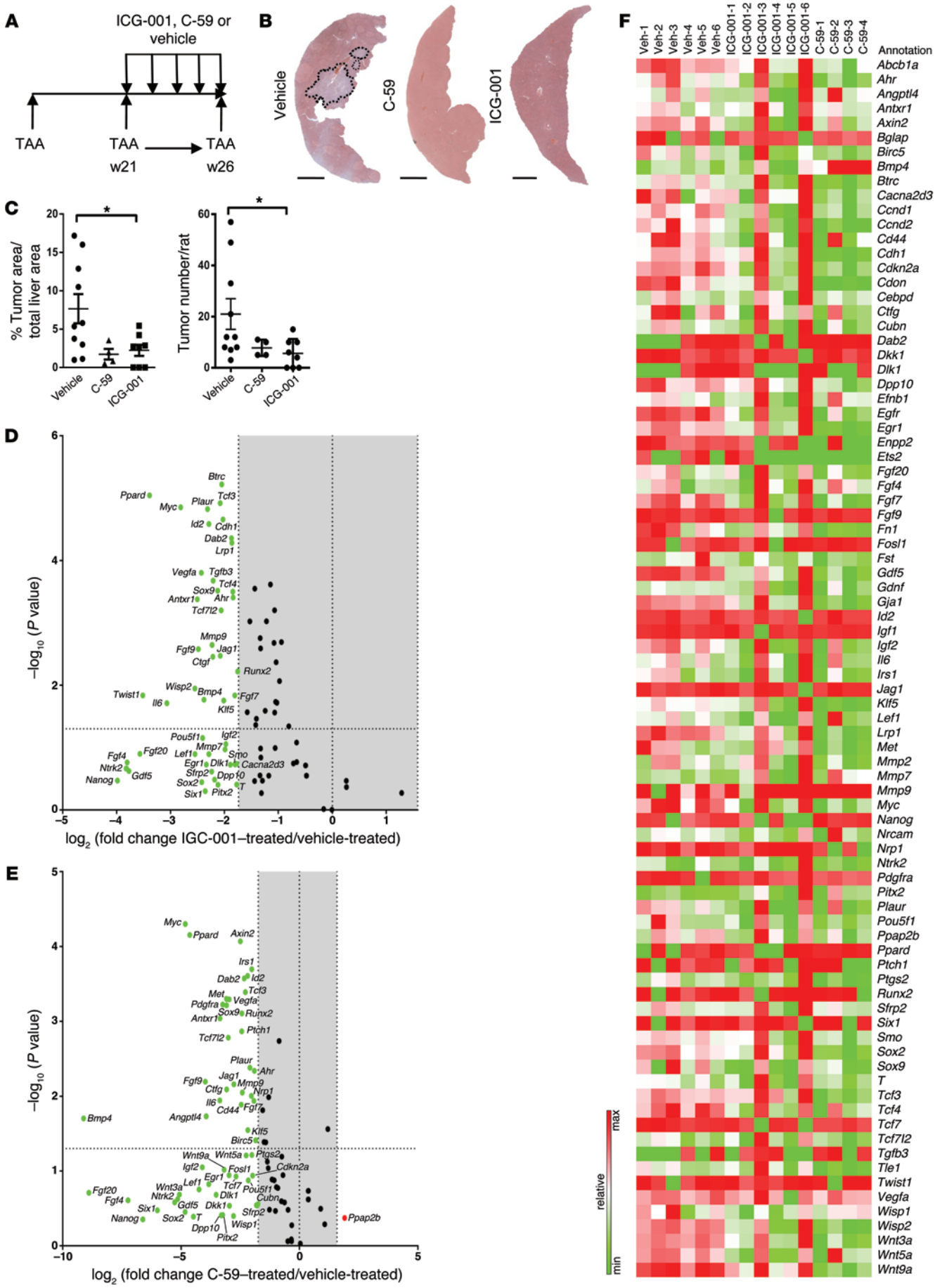
A
ICG-001, C-59 or vehicle
TAA
TAA
w21
TAA
w26
B
Vehicle
C-59
ICG-001
C
% Tumor area/ total liver area
Tumor number/rat
Vehicle
C-59
ICG-001
D
−log10 (P value)
log2 (fold change IGC-001–treated/vehicle-treated)
E
−log10 (P value)
log2 (fold change C-59–treated/vehicle-treated)
F
Veh-1
Veh-2
Veh-3
Veh-4
Veh-5
Veh-6
ICG-001-1
ICG-001-2
ICG-001-3
ICG-001-4
ICG-001-5
ICG-001-6
C-59-1
C-59-2
C-59-3
C-59-4
Annotation
relative
max
min

Figure 8. Inhibition of the canonical WNT signaling pathway reduces CC in vivo. (**A**) Schematic representing WNT inhibition in the TAA CC model. (**B**) H&E of TAA CC treated with vehicle, C-59, or ICG-001. (**C**) Quantification of tumor area and number in TAA CC following treatment with vehicle (n = 10), C-59 (n = 4), or ICG-001 (n = 8). (**D**) mRNA expression of WNT targets in TAA CC following treatment with ICG-001 (n = 6 in both groups). Data are presented as 3-fold change; $P < 0.05$; green, downregulation. (**E**) mRNA expression of WNT targets in TAA CC following treatment with C-59. Data are presented 3-fold change; $P < 0.05$; green, downregulation; red, upregulation (n = 6 in vehicle and n = 4 in C-59). (**F**) Heat map comparing expression of individual samples treated with vehicle, ICG0-001, or C-59. Data are presented as mean ± SEM. Kruskal-Wallis test; $^*P < 0.05$. Scale bars: 5 mm.

through the transcription of a broad panel of target genes that have been implicated in cell cycle transition, mitotic spindle assembly, and DNA segregation (57–61). However, the function of WNT signaling in both homeostasis and tumorigenesis is not simple, as WNT signaling appears to have different functions at different signaling levels, and so the well-described on-off model of WNT signaling is unlikely to be borne out in complex cellular environments (36, 62). Understanding how the WNT signaling cascade is regulated in a complex cellular environment, where multiple cellular components will influence the growth of the cancer and WNT activity, will be important for the development of therapeutic approaches to the treatment of WNT-dependent cancers.

CC represents an increasingly prevalent global challenge and remains untreatable. In many other malignancies where the WNT pathway activation is a hallmark of disease progression, blockade of the canonical WNT signal has failed as standard-of-care treatment, with tumors being refractory to these new WNT inhibitors. The WNT signaling pathway is complex and has multiple nodes of interaction with other signaling cascades. Because of this, WNT signaling sits in a highly regulated hierarchy in which it is influenced by both auto-regulatory and para-regulatory signals. There has been a large body of work to explain why these recombinant protein or small molecule approaches have failed to achieve clinical impact. In general, lack of responsiveness can be largely explained by mutations in core elements of the canonical WNT pathway such as CTNNB1 or APC, which function downstream of many canonical inhibitors and represent one of the most frequently mutated complexes in multiple cancer types (3, 63, 64). While knowing the common mutation profiles allows drug discovery and compound development to be focused for these tumors, it is important to also recognize that the presence of mutations in core pathway components does not mean that that pathway is critical for tumor growth per se.

Recent exome sequencing on human CC from both spontaneous and fluke-associated CC has identified multiple mutated candidates that could act as drivers in CC (6, 31). Of note is that RNF43, an E3 ligase required for normal FZD receptor turnover following ligand binding, is regularly mutated in fluke-associated CC, but not in spontaneous CC (31). Interestingly, and unlike other gastrointestinal cancers such as hepatocellular carcinoma (HCC) and colon cancer, the *CTNNB1* and *APC* loci are infrequently mutated, indicating CC could be susceptible to WNT inhibitor–based therapies, as there are no commonly described mutations downstream of the point of inhibition (i.e., APC or CTNNB1) that would allow these tumors to grow in a WNT ligand–independent manner.

Inflammatory macrophages in other systems have been shown to contribute to repair and carcinogenesis through the production of WNT ligands (9, 10). This process appears to be critical in the mediation of epithelial repair across a variety of organs, including kidney, liver, and colon (9, 10, 65). Importantly, and as also supported by our data, the role of WNT signaling in regeneration by macrophages appears to be orchestrated by M2 (alternatively activated) macrophages, which are able to stimulate the canonical WNT signaling cascade in colonic epithelial cells; however, M1 (classically activated) macrophages, in the colon at least, cannot (65). In a variety of diseased tissues and cancers, macrophage-derived WNT ligands play diverse roles and have been implicated in proliferation, inhibition of the autophagosome, and also metastasis (10, 65–67). The presence of certain monocyte subsets in CC has been correlated with a worse prognosis in CC (68), identifying the inflammatory milieu as a critical source of survival signals in CC growth.

In this study, we demonstrate a link between disease progression and WNT activation in human CC and both a mouse transgenic and chemically induced rat model, in which activation of the WNT signaling pathway correlated with growth of CC. More important, perhaps, we clearly show that inhibition of the canonical WNT pathway through inhibition of CTNNB1-CTBP signaling or indeed through inhibition of secretion of WNT ligand in vivo significantly reduces both tumor size and tumor number, revealing therapeutic WNT inhibition as a potential treatment for CC in humans.

Methods

Cell culture. CC-LP-1 and CC-SW-1 were provided by T.L. Whiteside, University of Pittsburgh, Pittsburgh, Pennsylvania, USA. WITT-1 donated by J.P. Iredale, MRC Centre for Inflammation Research (39, 40). SNU-1196 and SNU-1079 were purchased from the Korean Cell Line Bank (http://cellbank.snu.ac.kr/english/index.php). These cells were tested for the presence of mycoplasma in-house at the beginning of the study and were found to be negative. In this study cells were maintained in DMEM with glutamine and 5% FCS (PAA) at 37°C and with 5% CO_2. For in vitro cell viability assays, cells were plated at a density of $1 \times 10^4/cm^2$. All cell lines were treated for 5 days with ICG-001 (Tocris) or vehicle alone or 10 days with C-59 (Cellagen) inhibitor or vehicle alone at the concentrations shown in Figure 6 and Supplemental Figure 4. In experiments that were not dose response studies, cells were incubated with ICG-001 at 7.5 μM and C-59 at 100 nM. In these studies vehicle was always volume-matched DMSO. MTT assay was conducted using 3-(4,5-dimethylthiazol-2-yl)-2,5-diphenyltetrazolium bromide (5 mg/ml) (Sigma-Aldrich) diluted in PBS (Sigma-Aldrich). Cells were treated for 12 hours, and MTT crystals were dissolved in DMSO and read at 570/690 nm using a FluoStar Omega (BMG Labtech). BrdU incorporation assay (Cell Signaling Technology) and caspase-3/7 activity assays (Promega) were conducted as described in the manufacturer's instructions.

Human tissue was collected under approval of the University of Edinburgh ethics committee and diagnosed by the NHS Lothian/University of Edinburgh Pathology Department. Healthy liver was provided by the NRS BioResource, NHS Lothian. All tissues were collected with informed consent. Tissue microarrays (TMAs)–tissue block LVC1261 were purchased from Pantomics.

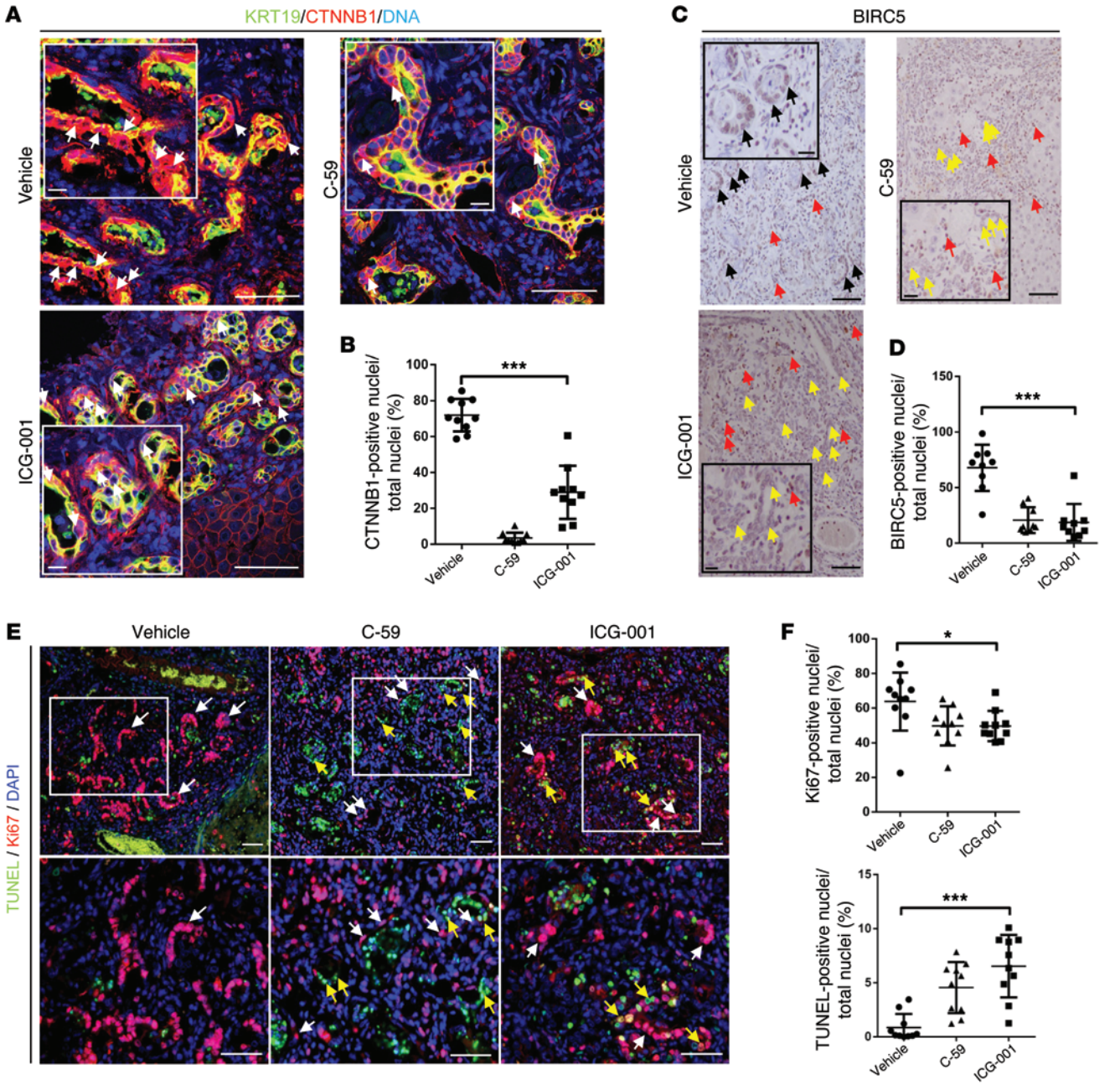

Figure 9. Loss of WNT signaling reduces proliferation and induces apoptosis in CC in vivo. (**A**) Immunohistochemistry for KRT19 (green) and CTNNB1 (red) in TAA CC treated with vehicle, C59, or ICG-001. White arrows, nuclear positivity for CTNNB1. (**B**) Quantification of nuclear CTNNB1 staining in TAA CC following treatment with vehicle C-59 or ICG-001 (n = 10 per group). (**C**) Immunohistochemistry for BIRC5 in TAA CC following treatment with vehicle, C-59, or ICG-001 (black arrows, nuclear positivity for BIRC5 in epithelium; red, non-epithelial BIRC5 positivity; yellow, epithelium negative for BIRC5). (**D**) Quantification of epithelial BIRC5 positivity following treatment with vehicle, C-59, or ICG-001 (n = 10 per group). (**E**) Immunohistochemistry for TUNEL (green) and Ki-67 (red) in TAA CC treated with vehicle, C-59, or ICG-001. White boxes, regions magnified in lower panels; white arrows, epithelial positivity for Ki-67; yellow arrows, epithelial positivity for TUNEL. (**F**) Quantification of Ki-67 and TUNEL staining in CC epithelial nuclei following treatment with vehicle, C-59, or ICG-001 (n = 10 per group). Data are presented as mean ± SEM. Kruskal-Wallis test; $^*P < 0.05$, $^{***}P < 0.001$. Scale bars: 50 μm; inset, 10 μm.

Animal studies. All animal work was conducted in accordance with the UK Home Office regulations. Animals were housed in 12-hour light/12-hour dark cycles and were given access to food and water ad libitum. The number of animals used in each experiment was calculated based on an α value of 0.05 and a power of 0.90 using data from either pilot studies or based on previous work.

Human ICC xenograft models. Male CD1 nude mice (Harlan) were injected subcutaneously with 5×10^5 human ICC cells from human cell line WITT-1, CC-LP-1, or SNU-1079 (n = 24 in all cases) suspended in culture media/RGF Matrigel (Gibco) mix (1:1). Cells were engrafted bilaterally in the flank and allowed to form tumors over 3 weeks. Once palpable tumors had formed, mice were randomized into

3 groups using GraphPad online software (http://www.graphpad.com/quickcalcs/ramdomize1.cfm). Xenografted mice were injected with liposomal clodronate at 4 μl/g intravenously (ClodronateLiposomes.org). The control for this treatment was saline alone or liposomes not containing clodronate (both given at 4 μl/g intravenously). All of these treatments were given every 48 hours for 3 weeks. We excluded it, however, from gene expression analysis. CSFR1 inhibitors AZD7507 (AstraZeneca) and GW2580 (LC Laboratories) were made up in sterile water containing 0.5% methylcellulose and 0.1% Tween-80. AZD7507 was given twice daily at 100 mg/kg, whereas GW2580 was given daily at 160 mg/kg. Control animals were given water containing 0.5% methylcellulose (Sigma-Aldrich) and 0.1% Tween-80 (Sigma-Aldrich). ICG-001 (5 mg/kg) (Tocris) or C-59 (20 mg/kg) (Cellagen) was given by intraperitoneal injection. The vehicle for this was physiological saline (Sigma-Aldrich). Control animals were given vehicle alone. In all cases inhibitors and vehicle were given 3 times per week.

TAA mouse tumor models. Male *Krt19-CreER^T R26R-eYFP p53$^{fl/fl}$*, *Krt19-CreER^T R26R-eYFP p53$^{fl/WT}$*, and *Krt19-CreER^T R26R-eYFP p53$^{WT/WT}$* mice were given 3 injections of 4 mg tamoxifen (Sigma-Aldrich) i.p. and then given TAA (Sigma-Aldrich) (600 mg/l) in sweetened water for 26 weeks.

TAA rat tumor models. Male Sprague-Dawley rats were given TAA (Sigma-Aldrich) in sweetened water for 26 weeks at a concentration of 600 mg/l. At 21 weeks rats were randomized into groups using GraphPad online software and were injected with liposomal clodronate at 4 μl/g (ClodronateLiposomes.org). The control for this treatment was saline alone or liposomes not containing clodronate (both given at 4 μl/g). There is increasing evidence that the latter control is inappropriate, as liposomes themselves alter the phenotype of macrophages (ClodronateLiposomes.org and ref. 38). We have included this group in our tumor volume and mass quantification. ICG-001 (5 mg/kg) (Tocris) or C-59 (20 mg/kg) (Cellagen) was given by i.p. injection. The vehicle for this was physiological saline (Sigma-Aldrich). Control animals were given vehicle alone. In all cases inhibitors and vehicle were given 3 times per week.

Immunohistochemistry. Tissue was perfused with PBS, dissected, and then fixed in 10% buffered formalin for 12 hours and dehydrated. Tissue sections were cut at 4 μm. Briefly, sections were de-waxed in xylene and rehydrated through graduated alcohol. Sections were subject to heat-mediated antigen retrieval followed by blocking using a protein block (Vector Biolabs). Sections were incubated overnight with primary antibodies at 4°C. After washing, sections were stained with species-appropriate secondary antibodies conjugated to Alexa 488, Alexa 555 (all from Life Biosciences), or Biotin (Vector). For colorimetric stains, sections were incubated with ABC reagent (Vector Biolabs) and developed using DAB (Vector). For a complete list of primary antibodies, see Supplemental Table 6. Positive control immunohistochemistry tissue (E11.5 mouse sagittal sections) was provided by Rachel Berry, MRC Human Genetics Unit, Edinburgh, UK. All confocal images were taken using the Leica SP2 TCS system and were deconvoluted using Fiji ImageJ (EMBL); non-confocal fluorescence and transmitted light were photographed using a Nikon Eclipse E400 system.

Gene expression analysis. Cells and tissues were lysed into TriReagent (Ambion) and homogenized using a tissue tearer. Lysates were mixed with 1:5 chloroform/TriReagent and spun for 15 minutes. The aqueous phase containing RNA was collected, and RNA was precipitated using isopropanol. The precipitate was applied to an RNeasy Mini column (QIAGEN), and the manufacturer's protocol was followed. Isolated RNA was quantified using a NanoDrop 1000, and then 1 μg was reverse transcribed using the Quantitect RT kit (QIAGEN) as per the manufacturer's instructions. 25 ng of cDNA was assayed using SYBRfast qPCR reagents and Quantifast primers from QIAGEN. For a complete list of primers, see Supplemental Table 6. All analysis was conducted using a LightCycler 480-II (Roche). qPCR pathway arrays were purchased from SABiosciences and were used as per the manufacturer's protocol.

Statistics. Quantification of xenograft size was performed in a blinded manner, and size of tumors in vivo was performed as a double-blind analysis by an independent clinically trained pathologist. For quantification of TMA core in human samples, the whole biopsy core was photographed in a blinded fashion and counted. For quantification of rat tissue, 10 pathologically discrete tumors were selected, imaged in their entirety, and counted in blinded fashion. All experimental groups were analyzed for normality using a D'Agostino-Pearson omnibus test. Groups that were normally distributed were compared with either a 2-tailed Student's *t* test (for analysis of 2 groups) or using 1-way ANOVA to compare multiple groups. Non-parametric data were analyzed using a Wilcoxon–Mann-Whitney *U* test when comparing 2 groups or a Kruskal-Wallis test when comparing multiple non-parametric data. Throughout, $P < 0.05$ was considered significant. $^*P < 0.05$, $^{**}P < 0.01$, $^{***}P < 0.001$. Data are presented as mean with SEM for parametric data or median with SD for non-parametric data.

Study approval. All studies involving human tissue were approved by the University of Edinburgh and NHS Lothian Academic and Clinical Central Office for Research Development (ACCORD) tissue governance unit. All tissue was collected with informed consent. Animal studies were approved by the University of Edinburgh Animal Welfare and Ethical Review Body (AWERB) and licensed by the UK Home Office.

Acknowledgments

L. Boulter is funded by the Medical Research Council (G1000868/97900), Cancer Research UK (C26848/A14889), and the Alan Morement Memorial Fund. S.J. Forbes is funded by the Medical Research Council (G1000868/97900), Cancer Research UK (C26848/A14889), the Alan Morement Memorial Fund, and UK Regenerative Medicine Platform (MR/M007588/1). A.J. Robson is funded by a personal MRC fellowship, and O.J. Sansom is funded by Cancer Research UK and the European Research Council. R.V. Guest and T.J. Kendall are funded by personal Wellcome Trust fellowships. Clodronate (Cl_2MDP) was a gift from Roche Diagnostics. We thank the NRS BioResource for provision of human tissue and Rachel Berry for provision of embryonic tissue, Robert Walker for technical assistance, and E.M.J. Boulter-Comer for proofreading of the manuscript.

Address correspondence to: Stuart J. Forbes, MRC Centre for Regenerative Medicine, 5 Little France Drive, Edinburgh, EH16 4UU, United Kingdom. Phone: 44.0.131.651.9500; E-mail: stuart.forbes@ed.ac.uk.

1. Barker N, et al. Crypt stem cells as the cells-of-origin of intestinal cancer. *Nature*. 2009;457(7229):608–611.
2. Mo ML, Li MR, Chen Z, Liu XW, Sheng Q, Zhou HM. Inhibition of the Wnt palmitoyltransferase porcupine suppresses cell growth and down-regulates the Wnt/β-catenin pathway in gastric cancer. *Oncol Lett*. 2013;5(5):1719–1723.
3. Kahn M. Can we safely target the WNT pathway? *Nat Rev Drug Discov*. 2014;13(7):513–532.
4. Khan SA, Taylor-Robinson SD, Toledano MB, Beck A, Elliott P, Thomas HC. Changing international trends in mortality rates for liver, biliary and pancreatic tumours. *J Hepatol*. 2002;37(6):806–813.
5. Njei B. Changing pattern of epidemiology in intrahepatic cholangiocarcinoma. *Hepatology*. 2014;60(3):1107–1108.
6. Ong CK, et al. Exome sequencing of liver fluke-associated cholangiocarcinoma. *Nat Genet*. 2012;44(6):690–693.
7. Tokumoto N, et al. Immunohistochemical and mutational analyses of Wnt signaling components and target genes in intrahepatic cholangiocarcinomas. *Int J Oncol*. 2005;27(4):973–980.
8. Zhang KS, Zhou Q, Wang YF, Liang LJ. Inhibition of Wnt signaling induces cell apoptosis and suppresses cell proliferation in cholangiocarcinoma cells. *Oncol Rep*. 2013;30(3):1430–1438.
9. Boulter L, et al. Macrophage-derived Wnt opposes Notch signaling to specify hepatic progenitor cell fate in chronic liver disease. *Nat Med*. 2012;18(4):572–579.
10. Lin SL, et al. Macrophage Wnt7b is critical for kidney repair and regeneration. *Proc Natl Acad Sci U S A*. 2010;107(9):4194–4199.
11. Loilome W, et al. Activated macrophages promote Wnt/β-catenin signaling in cholangiocarcinoma cells. *Tumour Biol*. 2014;35(6):5357–5367.
12. Guest RV, et al. Cell lineage tracing reveals a biliary origin of intrahepatic cholangiocarcinoma. *Cancer Res*. 2014;74(4):1005–1010.
13. Yeh CN, Maitra A, Lee KF, Jan YY, Chen MF. Thioacetamide-induced intestinal-type cholangiocarcinoma in rat: an animal model recapitulating the multi-stage progression of human cholangiocarcinoma. *Carcinogenesis*. 2004;25(4):631–636.
14. Ling H, et al. Transforming growth factor β neutralization ameliorates pre-existing hepatic fibrosis and reduces cholangiocarcinoma in thioacetamide-treated rats. *PLoS One*. 2013;8(1):e54499.
15. Praet MM, Roels HJ. Histogenesis of cholangiomas and cholangiocarcinomas in thioacetamide fed rats. *Exp Pathol*. 1984;26(1):3–14.
16. Yeh CN, et al. cDNA microarray pro fi ling of rat cholangiocarcinoma induced by thioacetamide. *Mol Med Rep*. 2013;8(2):350–360.
17. Yeh CN, et al. Animal PET for thioacetamide-induced rat cholangiocarcinoma: a novel and reliable platform. *Mol Imaging Biol*. 2008;10(4):209–216.
18. Li Q, et al. Disruption of Klf4 in villin-positive gastric progenitor cells promotes formation and progression of tumors of the antrum in mice. *Gastroenterology*. 2012;142(3):531–542.
19. Yu F, et al. Kruppel-like factor 4 (KLF4) is required for maintenance of breast cancer stem cells and for cell migration and invasion. *Oncogene*. 2011;30(18):2161–2172.
20. Furuyama K, et al. Continuous cell supply from a Sox9-expressing progenitor zone in adult liver, exocrine pancreas and intestine. *Nat Genet*. 2011;43(1):34–41.
21. Morita Y, et al. Expression of urokinase-type plasminogen activator receptor in hepatocellular carcinoma. *Hepatology*. 1997;25(4):856–861.
22. Takeha S, Fujiyama Y, Bamba T, Sorsa T, Nagura H, Ohtani H. Stromal expression of MMP-9 and urokinase receptor is inversely associated with liver metastasis and with infiltrating growth in human colorectal cancer: a novel approach from immune/inflammatory aspect. *Jpn J Cancer Res*. 1997;88(1):72–81.
23. McGraw HF, Culbertson MD, Nechiporuk AV. Kremen1 restricts Dkk activity during posterior lateral line development in zebrafish. *Development*. 2014;141(16):3212–3221.
24. Burke ZD, Reed KR, Phesse TJ, Sansom OJ, Clarke AR, Tosh D. Liver zonation occurs through a β-catenin-dependent, c-Myc-independent mechanism. *Gastroenterology*. 2009;136(7):2316–2324.
25. Takada K, et al. Targeted disruption of the BCL9/beta-catenin complex inhibits oncogenic Wnt signaling. *Sci Transl Med*. 2012;4(148):148ra117.
26. Fiedler M, et al. Decoding of methylated histone H3 tail by the Pygo-BCL9 Wnt signaling complex. *Mol Cell*. 2008;30(4):507–518.
27. Thompson B, Townsley F, Rosin-Arbesfeld R, Musisi H, Bienz M. A new nuclear component of the Wnt signalling pathway. *Nat Cell Biol*. 2002;4(5):367–373.
28. Townsley FM, Cliffe A, Bienz M. Pygopus and Legless target Armadillo/β-catenin to the nucleus to enable its transcriptional co-activator function. *Nat Cell Biol*. 2004;6(7):626–633.
29. Conacci-Sorrell M, Ngouenet C, Anderson S, Brabletz T, Eisenman RN. Stress-induced cleavage of Myc promotes cancer cell survival. *Genes Dev*. 2014;28(7):689–707.
30. Conacci-Sorrell M, Ngouenet C, Eisenman RN. Myc-nick: a cytoplasmic cleavage product of Myc that promotes alpha-tubulin acetylation and cell differentiation. *Cell*. 2010;142(3):480–493.
31. Chan-On W, et al. Exome sequencing identifies distinct mutational patterns in liver fluke-related and non-infection-related bile duct cancers. *Nat Genet*. 2013;45(12):1474–1478.
32. de Lau W, et al. Lgr5 homologues associate with Wnt receptors and mediate R-spondin signalling. *Nature*. 2011;476(7360):293–297.
33. Ruffner H, et al. R-Spondin potentiates Wnt/β-catenin signaling through orphan receptors LGR4 and LGR5. *PLoS One*. 2012;7(7):e40976.
34. Wang D, Huang B, Zhang S, Yu X, Wu W, Wang X. Structural basis for R-spondin recognition by LGR4/5/6 receptors. *Genes Dev*. 2013;27(12):1339–1344.
35. Xu K, Xu Y, Rajashankar KR, Robev D, Nikolov DB. Crystal structures of Lgr4 and its complex with R-spondin1. *Structure*. 2013;21(9):1683–1689.
36. de Lau W, Peng WC, Gros P, Clevers H. The R-spondin/Lgr5/Rnf43 module: regulator of Wnt signal strength. *Genes Dev*. 2014;28(4):305–316.
37. Schulz C, et al. A lineage of myeloid cells independent of Myb and hematopoietic stem cells. *Science*. 2012;336(6077):86–90.
38. Ramachandran P, et al. Differential Ly-6C expression identifies the recruited macrophage phenotype, which orchestrates the regression of murine liver fibrosis. *Proc Natl Acad Sci U S A*. 2012;109(46):E3186–E3195.
39. Shimizu Y, et al. Two new human cholangiocarcinoma cell lines and their cytogenetics and responses to growth factors, hormones, cytokines or immunologic effector cells. *Int J Cancer*. 1992;52(2):252–260.
40. Harnois DM, Que FG, Celli A, LaRusso NF, Gores GJ. Bcl-2 is overexpressed and alters the threshold for apoptosis in a cholangiocarcinoma cell line. *Hepatology*. 1997;26(4):884–890.
41. Van Rooijen N, Sanders A. Kupffer cell depletion by liposome-delivered drugs: comparative activity of intracellular clodronate, propamidine, and ethylenediaminetetraacetic acid. *Hepatology*. 1996;23(5):1239–1243.
42. Conway JG, et al. Effects of the cFMS kinase inhibitor 5-(3-methoxy-4-((4-methoxybenzyl) oxy)benzyl)pyrimidine-2,4-diamine (GW2580) in normal and arthritic rats. *J Pharmacol Exp Ther*. 2008;326(1):41–50.
43. Conway JG, et al. Inhibition of colony-stimulating-factor-1 signaling in vivo with the orally bioavailable cFMS kinase inhibitor GW2580. *Proc Natl Acad Sci U S A*. 2005;102(44):16078–16083.
44. Scott DA, et al. Mitigation of cardiovascular toxicity in a series of CSF-1R inhibitors, and the identification of AZD7507. *Bioorg Med Chem Lett*. 2013;23(16):4591–4596.
45. Li J, et al. Biliary repair and carcinogenesis are mediated by IL-33-dependent cholangiocyte proliferation. *J Clin Invest*. 2014;124(7):3241–3251.
46. Herr P, Basler K. Porcupine-mediated lipidation is required for Wnt recognition by Wls. *Dev Biol*. 2012;361(2):392–402.
47. Henderson WR, et al. Inhibition of Wnt/β-catenin/CREB binding protein (CBP) signaling reverses pulmonary fibrosis. *Proc Natl Acad Sci U S A*. 2010;107(32):14309–14314.
48. Barrott JJ, Cash GM, Smith AP, Barrow JR, Murtaugh LC. Deletion of mouse Porcn blocks Wnt ligand secretion and reveals an ectodermal etiology of human focal dermal hypoplasia/Goltz syndrome. *Proc Natl Acad Sci U S A*. 2011;108(31):12752–12757.
49. Biechele S, Cockburn K, Lanner F, Cox BJ, Rossant J. Porcn-dependent Wnt signaling is not required prior to mouse gastrulation. *Development*. 2013;140(14):2961–2971.
50. Eguchi M, Nguyen C, Lee SC, Kahn M. ICG-001, a novel small molecule regulator of TCF/β-catenin transcription. *Med Chem*. 2005;1(5):467–472.
51. Wend P, et al. Wnt/β-catenin signalling induces MLL to create epigenetic changes in salivary gland tumours. *EMBO J*. 2013;32(14):1977–1989.
52. Gang EJ, et al. Small-molecule inhibition of CBP/catenin interactions eliminates drug-resistant clones in acute lymphoblastic leukemia. *Oncogene*. 2014;33(17):2169–2178.
53. Proffitt KD, et al. Pharmacological inhibition of the Wnt acyltransferase PORCN prevents growth of WNT-driven mammary cancer. *Cancer Res*. 2013;73(2):502–507.
54. Ku JL, et al. Establishment and characterisation of six human biliary tract cancer cell lines. *Br J*

Cancer. 2002;87(2):187–193.
55. Liu J, et al. Targeting Wnt-driven cancer through the inhibition of Porcupine by LGK974. *Proc Natl Acad Sci U S A*. 2013;110(50):20224–20229.
56. Wang X, et al. The development of highly potent inhibitors for porcupine. *J Med Chem*. 2013;56(6):2700–2704.
57. Mbom BC, Siemers KA, Ostrowski MA, Nelson WJ, Barth AI. Nek2 phosphorylates and stabilizes β-catenin at mitotic centrosomes downstream of Plk1. *Mol Biol Cell*. 2014;25(7):977–991.
58. Mbom BC, Nelson WJ, Barth A. β-Catenin at the centrosome: discrete pools of beta-catenin communicate during mitosis and may co-ordinate centrosome functions and cell cycle progression. *Bioessays*. 2013;35(9):804–809.
59. Acebron SP, Karaulanov E, Berger BS, Huang YL, Niehrs C. Mitotic wnt signaling promotes protein stabilization and regulates cell size. *Mol Cell*. 2014;54(4):663–674.
60. Dutta-Simmons J, et al. Aurora kinase A is a target of Wnt/beta-catenin involved in multiple myeloma disease progression. *Blood*. 2009;114(13):2699–2708.
61. Luis TC, et al. Wnt3a deficiency irreversibly impairs hematopoietic stem cell self-renewal and leads to defects in progenitor cell differentiation. *Blood*. 2009;113(3):546–554.
62. Buchert M, et al. Genetic dissection of differential signaling threshold requirements for the Wnt/β-catenin pathway in vivo. *PLoS Genet*. 2010;6(1):e1000816.
63. Lenz HJ, Kahn M. Safely targeting cancer stem cells via selective catenin coactivator antagonism. *Cancer Sci*. 2014;105(9):1087–1092.
64. McMillan M, Kahn M. Investigating Wnt signaling: a chemogenomic safari. *Drug Discov Today*. 2005;10(21):1467–1474.
65. Cosin-Roger J, et al. M2 macrophages activate WNT signaling pathway in epithelial cells: relevance in ulcerative colitis. *PLoS One*. 2013;8(10):e78128.
66. Wynn TA, Chawla A, Pollard JW. Macrophage biology in development, homeostasis and disease. *Nature*. 2013;496(7446):445–455.
67. Yeo EJ, et al. Myeloid WNT7b mediates the angiogenic switch and metastasis in breast cancer. *Cancer Res*. 2014;74(11):2962–2973.
68. Subimerb C, et al. Circulating CD14(+) CD16(+) monocyte levels predict tissue invasive character of cholangiocarcinoma. *Clin Exp Immunol*. 2010;161(3):471–479.